NACA RM L52H08a

RESEARCH MEMORANDUM

AN INVESTIGATION AT TRANSONIC SPEEDS OF THE AERODYNAMIC CHARACTERISTICS OF AN AIR INLET INSTALLED IN THE ROOT OF A 45° SWEPTBACK WING

By Robert R. Howell and Arvid L. Keith, Jr.

Langley Aeronautical Laboratory
Langley Field, Va.

NATIONAL ADVISORY COMMITTEE FOR AERONAUTICS

WASHINGTON

October 1, 1952

NATIONAL ADVISORY COMMITTEE FOR AERONAUTICS

RESEARCH MEMORANDUM

AN INVESTIGATION AT TRANSONIC SPEEDS OF THE AERODYNAMIC CHARACTERISTICS OF AN AIR INLET INSTALLED IN THE ROOT OF A 45° SWEPTBACK WING

By Robert R. Howell and Arvid L. Keith, Jr.

SUMMARY

An investigation has been made in the Langley transonic blowdown tunnel at Mach numbers from 0.80 to 1.41 to determine the increments in lift and drag due to installation of a triangular-shaped air inlet in the root of a 45° sweptback wing and to study the internal flow characteristics of the inlet. The test ranges of angle of attack and mass-flow ratio were from -2.0° to 8.2° and 0.34 to 0.77, respectively. Measurements included total pressures at the inlet and at an assumed engine compressor-face station and the lift and drag of the wing-body combination. A basic configuration was used for evaluating the increments in aerodynamic forces due to the inlet installation.

At a test mass-flow ratio of about 0.70 a total-pressure recovery of 90 percent or greater was obtained without a bypass scoop for all test angles of attack up to a Mach number of 1.20. Installation of a bypass scoop extended the Mach number range for a pressure recovery of 90 percent or greater to 1.36. The drag increment due to the bypass was small and a maximum estimated gain in thrust minus drag of 7.8 percent of the 100-percent pressure-recovery thrust was obtained at a Mach number of 1.41. The drag increment due to the inlet was small throughout the test ranges of mass-flow ratio and Mach number for angles of attack up to about 3°. At higher angles of attack the drag increment became appreciable in the Mach number range around 1.1, and then decreased with further increases in Mach number. The increment in lift due to the inlet was positive except at the highest angles of attack at the highest Mach numbers. In general, the lift increment caused by the inlet installation was approximately in proportion to the increase in wing area.

INTRODUCTION

The choice of an air inlet and induction system design for a turbojet-powered airplane is often influenced by the specific mission to be fulfilled by the aircraft in that the allocation of equipment or personnel within the aircraft fuselage may require the selection of a nose inlet, a fuselage scoop, or a wing-root type inlet. For any type of inlet, the total-pressure recovery at the engine and the airplane drag increment due to the inlet installation are important factors influencing the aircraft performance.

A sweptback triangular-shaped air inlet in the root of a 45° sweptback wing was developed in reference 1 and was shown to have good pressure recovery and drag characteristics at low speeds for wide ranges of inlet mass-flow ratio and angle of attack. The relative size of the inlet and wing-body was representative of that required for a single-engine turbojet-powered fighter aircraft assumed to be flying at a Mach number of 1.0 and at an altitude of 35,000 feet and to be operating at an inlet mass-flow ratio of approximately 0.8. In order to determine the aerodynamic characteristics of this inlet in the transonic speed range, an investigation has been conducted in the Langley transonic blowdown tunnel through a range of Mach number from 0.80 to 1.41 at a Reynolds number of approximately 6.5×10^6. The measurements included total pressures at the intake and at an assumed engine compressor face, and the lift and drag. An unducted configuration was used as a basis for evaluating the increments in aerodynamic forces due to installation of the inlet. One design of a fuselage boundary-layer scoop and bypass was tested on the inlet model during the course of the investigation.

SYMBOLS

C_{D_b}	basic model drag coefficient, Drag/q_oS
$\Delta C_{D_{ext}}$	increment in external drag coefficient due to installation of the inlet (see appendix)
C_{L_b}	basic model lift coefficient, Lift/q_oS
$\Delta C_{L_{ext}}$	increment in lift coefficient due to installation of the inlet (see appendix)

$\overline{H}/H_o$ integrated total-pressure recovery weighted by local mass flow, $\dfrac{\int_A \frac{\rho V}{\rho_o V_o}\left(\frac{H}{H_o}\right)dA}{\int_A \frac{\rho V}{\rho_o V_o}\,dA}$

$\dfrac{H - p_o}{H_o - p_o}$ impact pressure ratio

m_i/m_o mass-flow ratio, defined as the ratio of total internal mass flow to the mass flow through a free-stream tube equal in area to that of the inlet

A area

A_i projected minimum frontal area of both inlet openings

c local chord

$\overline{c}$ mean aerodynamic chord basic wing (4.462 inches)

D_{mi} measured drag of inlet model

D_{mb} measured drag of basic model

F frontal area of fuselage (7.07 square inches)

F_N net thrust

H total pressure

L_{mi} measured lift of inlet model

L_{mb} measured lift of basic model

M Mach number

m rate of internal mass flow

p static pressure

q dynamic pressure, $\frac{1}{2}\rho V^2$

R Reynolds number (based on mean aerodynamic chord of basic model)

S basic wing area (80.2 square inches)

t wing section thickness, expressed in percent c

u local velocity parallel to surface and inside boundary layer

U local velocity parallel to surface at outer edge of boundary layer

V velocity

X distance parallel to fuselage center line

Y distance perpendicular to a plane through wing chord

α angle of attack

Subscripts:

B base of cut-off fuselage with no jet exit

c compressor-face station

i inlet station

o free stream

s bypass scoop

T portion of fuselage tail removed to provide exit for internal flow

x jet exit station

MODEL CONFIGURATIONS

Basic model.- The basic model consisted of a wing of 45° quarter-chord sweep mounted with zero incidence in the midwing position on a fuselage of fineness ratio 6.7 (figs. 1 and 2). The wing (table I) was composed of NACA 64A008 airfoil sections in the streamwise direction and had an aspect ratio of 4.032, a taper ratio of 0.6, no twist and no dihedral. The basic fuselage was formed by rotating an NACA 65_2A015 airfoil section about its chord line. A second fuselage was

formed by replacing the nose section of the basic fuselage with a 20.4° included-angle cone, as shown in figure 3; the fineness ratio of this fuselage was 7.7. Unless otherwise noted, all data given are for the basic rounded fuselage nose.

Inlet model.- The size of the inlet relative to the fuselage $\left(\frac{A_i}{F} = 0.167\right)$ was chosen to handle the air-flow requirements of a representative single-engine jet airplane assumed to be flying at an altitude of 35,000 feet at a Mach number of 1.0 and mass-flow ratio of 0.8. The inlet configuration investigated was identical with that of the final inlet configuration developed at low speeds in reference 1.

Provision for installation of the inlet in the wing root was made by increasing the quarter-chord sweep of the basic wing in the inboard section to 55°, by increasing the thickness ratio of the inboard wing section linearly from 8 percent to 13 percent, and by increasing the chord. (See table I.) The resulting inboard sections were cut off along a line corresponding to the leading edge of the wing outboard of the inlet, and the inlet lips were faired around the triangular inlet shape from this new leading edge to the maximum thickness of the wing. The triangular-shaped fillets increased the wing area by 8 percent. As shown in table II, the triangular-shaped inlet was made asymmetrical to provide a thick upper lip, desirable for obtaining a high maximum lift coefficient. Lower-lip stagger X_s, defined as indicated in table II, was also incorporated to improve the internal flow characteristics at high angles of attack. Pertinent dimensions of the inlet are shown in table II. Elliptical ordinates were used for fairing the inner and outer inlet lips.

Inasmuch as the two inlets were assumed to admit the air flow for one engine, the internal ducting for each inlet was designed to undergo a transition from a triangular shape at the inlet plane to a semicircular shape and the two ducts to merge at the assumed face of the engine. This transition was made at nearly constant area $\left(\frac{A_c}{A_i} = 1.042\right)$ and formed S-shaped ducts as shown in figure 3; typical sections showing the duct-shape transition are also included in the figure. This ducting, of course, does not necessarily correspond to that required in an actual installation; if the airplane ducting incorporates more abrupt S-bends or more diffusion or both, the total-pressure recovery would not be expected to be equal to the presented experimental values. The duct rearward of the engine-face station was circular and led to an exit in the tail end of the fuselage. Three exit areas A_x/A_c of 1.0, 0.75, and 0.50 were provided to vary the internal flow rate, as shown in figure 3.

The shape of the inlet and internal ducting was revised for some of the tests in order to permit installation of a boundary-layer bypass scoop (fig. 4). This scoop was designed to improve the total-pressure-recovery characteristics of the configuration by removing the fuselage boundary layer ahead of the inlet. The scoop flow was discharged from the lower surface of the wing and the rear contour of the internal duct was rounded as shown in figure 4 to discharge the flow approximately parallel to the local flow over the wing. Installation of the scoop reduced the primary inlet area ratio $\left(\frac{A_i - A_s}{F}\right)$ to 0.145 and increased the engine-face area ratio $\left(\frac{A_c}{A_i - A_s}\right)$ to 1.200. The scoop-inlet area ratio (A_s/A_i) was 0.136.

APPARATUS AND INSTRUMENTATION

The basic and inlet models were sting-mounted in the tunnel. (See fig. 2.) The "normal sting" which was used for the present investigation, consisted of a yoke-type support attached to an internal two-component (lift and drag) strain-gage balance through recessed sections in the top and bottom of the inlet- and basic-model afterbodies. A sharp-edged splitter was mounted between the two arms of the yoke. The interference effects of the supports on the model forces and on the jet issuing from the fuselage-tail exit were determined by use of the "twin-tare-sting" setup (fig. 2). Two parallel arms of the tare sting were attached to the model wings at the 58.4-percent-semispan station through two-component strain-gage balances and the recessed model sections were faired to the original contour. Two sets of measurements were made with this arrangement: (1) with a dummy normal sting in place, but not touching the model, and (2) with the dummy normal sting removed. The difference between these two results was algebraically added to the results obtained with the model mounted on the normal sting.

The pressure-tube instrumentation of the inlet model included rakes of total- and static-pressure tubes in the inlet, at the assumed engine compressor-face station, and at the exit in addition to surface-pressure orifices distributed over the fuselage. The inlet instrumentation consisted of 17 total- and 2 static-pressure tubes distributed in the right inlet as shown in figure 5; an identical dummy pressure-tube rake was installed in the left inlet in attempts to avoid flow assymetry due to rake blockage. The engine face was instrumented with 18 total- and 2 static-pressure tubes arranged as shown in figure 5, so that the total-pressure recovery and mass flow for each duct could be determined separately. The exit-pressure rakes were varied from 12 total- and 3 static-pressure tubes with the minimum-area fuselage-tail opening to 16 total- and 3 static-pressure tubes with the maximum-area opening.

These exit rakes, installed for both the force and pressure tests, were mounted from the sting and were free from the model. For the tests with the boundary-layer scoop installed, a total- and a static-pressure tube were installed in the scoop duct to measure the scoop mass flow. The surface-pressure instrumentation for the inlet model consisted of six orifices installed in the fuselage nose along the horizontal center line from fuselage station 2.00 to 7.00 and five orifices installed in the fuselage tail along the horizontal center line, from station 14.60 to 17.16. The basic model surface-pressure instrumentation consisted of 5 orifices installed in the fuselage nose along the horizontal center line from station 0 to 5 and seven orifices installed in the fuselage tail from station 13.6 to 19.00.

The tests were conducted in the Langley transonic blowdown tunnel. This tunnel has an octagonal-shaped slotted test section which is 26 inches between flats. The test section periphery is 1/8 open due to the slots. The short operating period of the tunnel (of the order of 1/2 minute) required quick-acting instruments for recording the data. The force measurements were obtained by photographing self-balancing potentiometers, and all pressure data were recorded photographically using flight-type pressure recorders.

TESTS

Forces and pressures were measured in separate tests in order to eliminate interference effects of the internal-pressure tubing on the force measurements. Pressure tests were also made in two parts, with and without the inlet rakes installed, to avoid the total-pressure losses at the compressor-face station associated with the wake of the inlet rakes. The majority of tests for both models were conducted with the basic airfoil-nose fuselage installed. For several tests, roughness (0.005 to 0.007-inch-diameter carborundum grains) was installed on the round nose for a distance of 0.7 inch measured along the surface from the nose of the fuselage. Several tests were also made with the conical nose installed.

The range of test variables and their estimated maximum error and the estimated maximum error of the measured coefficients are presented in the following tables:

Variable	Range	Estimated max. error
M_o	0.80 to 1.41	±0.01
R	5.7×10^6 to 7.4×10^6	(a)
α	-2.0° to 8.2°	±0.1°
m_i/m_o	0.34 to 0.77	±0.01

[a]At any given Mach number, the maximum variation in Reynolds number was ±2.2 percent due to changes in the tunnel stagnation temperature.

Measured coefficients	Estimated max. error of coefficient
C_D	±0.001
C_L	±0.001
$\frac{H - p_o}{H_o - p_o}$	±0.005
$\frac{\overline{H}}{H_o}$ (weighted)	±0.01
$\frac{p - p_o}{H_o - p_o}$	±0.005

The probable errors of the above quantities would be expected to be lower than the values shown.

At supersonic speeds, there exists a Mach number range in which model nose shocks and expansion and compression waves reflected from the wind-tunnel walls intersect the model and cause differences in the measured aerodynamic characteristics compared to those obtained in free air. For the present model configurations, pressure distributions and schlieren photographs of the flow about the basic body of revolution indicated that the lower limit in Mach number for body intersection of the reflected bow shock was about 1.11. Below this Mach number the reflected wave was weak and reflected to the subsonic flow field at the model nose. The upper Mach number limit for

reflections in the region of the inlet was approximately 1.17. No pressure tests for the inlet model were conducted in this range. For all supersonic Mach numbers, reflections of expansion and compression waves intersected the models and the absolute values of the force coefficients obtained may not be equivalent to free-air values. At subsonic speeds the absolute values of the force coefficients may also be different from free-air values because of possible tunnel-wall effects due to the large ratio of model size to tunnel size; as indicated in reference 2, however, these effects are believed to be small. The more important effects of installation of the inlet in the wing root on the aerodynamic forces, however, can be evaluated from the differences in the lift and drag between the inlet and basic models.

In the present investigation, the mass-flow ratio was varied by cutting off the aft end of the fuselage at various positions. The measured forces of the inlet model, therefore, were affected by these various exit configurations. In order to determine a true evaluation of the force increments due to installation of the inlet alone, the measured inlet model forces were corrected for the effects of the various exit configurations by the method shown in the appendix. It should be mentioned here that the values of the external drag increment due to installation of the inlet as obtained by this method are the same as those obtained by the commonly used relation

$$\Delta D_{ext} = D_{mi} - \left[m(V_o - \overline{V}_x) - (\overline{p}_x - p_o)A_x\right] - \left[D_{mb} + (\overline{p}_B - p_o)A_B\right]$$

except for an adjustment to the drag of the inlet model which makes the pressure drag of its afterbody equal to that of the corresponding portion of the basic model. This correction removes from the drag increment the external drag effects due to the jet. For the preceding equation, D_{mb} is equal to the drag of the basic model having the fuselage afterbody cut off at a position corresponding to the exit location on the inlet model ($A_B = A_x$).

RESULTS AND DISCUSSION

Pressure Measurements of Inlet Model

Flow over fuselage nose.- Pressure distributions over the fuselage nose of the inlet model (fig. 6) and schlieren observations of the flow indicated that the local supersonic velocities attained over the nose always terminated in a shock ahead of the inlet. At Mach numbers above

1.0, an additional shock occurred at the model nose. For the round-nose fuselage, this shock was in the form of a detached bow wave and for the pointed nose was in the form of an attached conical shock at Mach numbers above about 1.04.

Flow in inlet.- Contours of constant impact-pressure ratio $\frac{H - p_o}{H_o - p_o}$ at the inlet measuring station are presented in figure 7 for representative mass-flow ratios, Mach numbers, and angles of attack. These data show that, at subsonic speeds, decreases in mass-flow ratio below a value of about 0.70 caused rapid thickening of the entering fuselage boundary layer. However, no reversed or separated flow occurred for any of the mass flows investigated at these subsonic speeds (fig. 8). Increases in Mach number at a mass-flow ratio of about 0.70 also caused rapid increases in boundary-layer thickness due to increases in the pressure rise across the inlet shock. At Mach numbers above about 1.05, flow separation occurred at the inlet due to interaction of the inlet shock and the fuselage boundary layer. Further increases in Mach number to 1.21 caused the separation to extend over a greater portion of the inlet and resulted in substantial losses in impact-pressure ratio. Decreases in mass-flow ratio at the higher Mach numbers caused a still greater region of separated flow (fig. 8) and consequently greater losses in impact-pressure ratio. It appeared that the exact Mach number at which boundary-layer separation began to occur was dependent upon both the mass-flow ratio and angle of attack. At an angle of attack of approximately 0°, total-pressure losses occurred in the region of the upper lip due to lip separation. (For example, see fig. 7 at $M_o = 1.02$ and $\frac{m_i}{m_o} = 0.69$.) No such local lip separation occurred at angles of attack above approximately 2° up to the maximum test angle. The greater losses at the lower inlet-lip–fuselage juncture as compared with those at the upper inlet-lip juncture at positive angles of attack might be alleviated somewhat by incorporating a generous fillet at the intersection. The preceding analysis indicates that the major portion of the inlet losses for flight conditions of practical interest are associated with the development of the boundary layer along the fuselage ahead of the inlet and the interaction of the shock ahead of the inlet with this boundary layer.

Flow at compressor face.- Contours of impact-pressure ratio at the compressor-face station (fig. 9) show that the losses at the compressor face were, in general, at the same relative location as those at the inlet measuring station. This fact is readily understood inasmuch as very little diffusion occurred between the two stations and, consequently, very little boundary-layer mixing and thickening took place in the duct.

At the lower test mass-flow ratios, the impact pressures indicated that flow asymmetry occurred between the two inlets. (For example, see fig. 9 at $M = 1.06$, $\alpha = 0.4^{\circ}$.) This asymmetry occurred for all test Mach numbers and angles of attack. An indication of the mass-flow ratio at which inlet flow asymmetry began to occur can be obtained from figure 10, where, for a representative angle of attack, individual inlet mass-flow ratios calculated from the pressures at the compressor-face station are plotted against system inlet mass-flow ratio determined at the model exit for several Mach numbers. This comparison shows that the asymmetrical flow between the two ducts began to occur at a system inlet mass-flow ratio of about 0.55. It is noted that this flow asymmetry was not of the type in which flow oscillations occur between two ducts, as indicated from time histories of the pressures, and also that the divergence of flow always occurred in the same direction. Although the mass-flow rate was never exactly the same in both ducts, probably because of asymmetrical blockage of the rake stem in the duct behind the compressor-face station, the differences from the mean were always about the same in the uniform flow range.

The effects of variations in free-stream Mach number, inlet mass-flow ratio, and angle of attack on the average total-pressure ratio $\bar{H}/H_0$ at the compressor-face station for the blunt-nose fuselage configuration are shown in figure 11. The total-pressure ratio rather than the impact-pressure ratio $\frac{H - p_0}{H_0 - p_0}$ is presented inasmuch as this parameter has the greater significance relative to the over-all airplane engine performance.

The total pressures at the lowest test Mach number (fig. 11(a)) never attained the free-stream value at any of the mass-flow ratios investigated because of losses of the entering fuselage boundary layer, skin friction in the ducts, and upper inlet-lip separation at the lowest angles of attack. The effect of increasing the Mach number was to reduce the total pressures for every flow condition and model attitude. The loss of total-pressure ratio caused by direct shock losses is shown in figure 11(a). This curve was calculated by assuming that the portions of the shocks ahead of the inlet through which the internal flow passes were normal shocks. It appears that, for the majority of mass-flow and angle-of-attack conditions, the total-pressure recovery decreased with Mach number at a greater rate than that indicated from the estimated shock losses at a Mach number greater than about 1.05. As discussed in the previous section, the increased losses were caused by fuselage boundary layer and boundary-layer–shock interaction effects.

Cross plots of the average total-pressure ratio at the compressor face as a function of angle of attack (fig. 11(b)) show that reductions in angle of attack below 2° brought about a slight decrease in total-pressure recovery. These losses were caused by separation from the

outboard region of the upper internal lip. (See fig. 7.) For all positive angles of attack, the total-pressure ratio was 0.90 or greater at a mass-flow ratio of 0.70 through the range of Mach number up to 1.20 (fig. 11(a)), and, at an angle of attack typical for high-speed flight ($\alpha = 4.4^{\circ}$, $C_L \approx 0.3$), the range of $\frac{\bar{H}}{H_o} \geq 0.90$ was extended to a Mach number of approximately 1.25 at the same mass-flow ratio.

The low total-pressure ratios obtained at the minimum mass-flow ratio of 0.40 (fig. 11(c)) were caused by losses which were associated with inlet flow asymmetry. The points making up the curves at this mass-flow ratio were obtained by integrating the total pressures over both halves of the compressor face and, consequently, contain the losses in the low mass-flow side $\left(\frac{m_i}{m_o} \approx 0.20\right)$ and the losses in the high mass-flow side $\left(\frac{m_i}{m_o} \approx 0.60\right)$. The losses presented for an average mass-flow ratio of 0.40, therefore, may not be representative of the losses for symmetrical flow conditions at the same mass-flow ratio. It should also be noted, however, that, although asymmetry existed, a total-pressure ratio of 0.90 or greater was obtained up to the design Mach number of 1.0 at the lowest test mass-flow ratio over the entire range of angle of attack (figs. 11(b) and (c)).

Increases in mass-flow ratio brought about significant increases in the total-pressure ratio for all Mach numbers; at a Mach number of 1.2 and angle of attack of 0.4°, the total-pressure ratio was increased from 0.82 at $\frac{m_i}{m_o} = 0.40$ to 0.90 at $\frac{m_i}{m_o} = 0.70$. It is believed that this trend would continue to mass-flow ratios higher than the maximum test value because of a reduction in the pressure rise acting on the boundary layer behind the shock. At least, the total-pressure ratios should not be less than the present maximum values up to the limiting mass-flow ratio. With the assumption of uniform inlet flow and use of the trends of total-pressure recovery with mass-flow ratio, the limiting mass-flow ratio at a Mach number of 1.4 was estimated to be at least 0.95. At lower supersonic speeds the limiting mass-flow ratio would be slightly greater than 0.95.

Force Measurements of Basic and Inlet Models

The force coefficients presented in this section of the paper are the lift and drag coefficients of the basic model and these coefficients plus the lift- and drag-coefficient increments due to installation of the inlet as determined by the method given in the appendix. All force

coefficients were based on the basic model wing area. The actual increase in wing area due to installation of the inlet, considering only the external triangular-shaped fillets, amounted to 8 percent of the basic wing area.

External drag.- External drag coefficients for the basic model and those for the basic model plus the drag increments due to the inlet with the inlet operating at a mass-flow ratio of 0.70 are presented in figure 12(a) as a function of Mach number for the several test angles of attack. In general, installation of the inlet caused no important increase in the external drag for the test range of Mach number at angles of attack up to about 3°. In fact, in the subsonic Mach number range, small reductions apparently occurred because of installation of the inlet. These apparent reductions could possibly be accounted for by a combination of the following: (1) the error in drag coefficient (maximum error in coefficient estimated to be ±0.001); (2) incorporation of a part of the fuselage nose skin-friction drag as internal drag (skin-friction drag coefficient of entering flow estimated to be 0.0008); and (3) a reduction in pressure drag due to the inlet installation. The low-speed tests of reference 1 also showed a reduction in drag at positive lift coefficients and inlet-velocity ratios above about 0.80. The reductions, however, were not as great as those indicated in the present investigation.

Increases in angle of attack above about 3° caused no significant changes in the drag increment due to the inlet at the lower test speeds. In the range of the peak drag (about $M_o = 1.1$), however, substantial drag increases were caused by the inlet. These increases reached a maximum at an angle of attack of approximately 6°. In evaluating the significance of these increments, it should be remembered that the inlet installation increased the wing area by 8 percent.

For the test Mach numbers above the peak drag, the drag increments due to the inlet became smaller than at the peak drag, and the trends of the curves indicate that the drag due to the inlet installation may be small at moderate as well as at low angles of attack for Mach numbers somewhat greater than the maximum test value.

The variations in drag coefficient with mass-flow ratio (fig. 12(c)) indicate that some reductions in the drag increment due to the inlet could be expected at mass-flow ratios greater than the maximum test value. Inasmuch as the total-pressure data of figure 11 showed increasing recovery with increasing mass flow, it is believed that the optimum inlet performance at transonic and supersonic speeds would be obtained at mass-flow ratios approaching 1.0.

Lift.- Lift coefficients for the basic model and those for the basic model plus the lift increments due to the inlet with the inlet operating

at a mass-flow ratio of 0.70 are presented in figure 13(a) as a function of Mach number for the several angles of attack. For the major portion of the test range, the lift increment due to the inlet was positive by an amount approximately in proportion to the increase in exposed wing area. For the highest test Mach number, highest angle of attack condition, small decreases in lift increment occurred probably because of local shock-induced separation in the root sections of the wing. These small changes in lift increment due to the inlet could possibly result in changes in pitching-moment characteristics at the high Mach number, high-angle-of-attack condition. The low-speed lift data of reference 1, however, show that installation of the inlet has a negligible effect on the lift characteristics up to angles of attack as high as 30°. Variations in mass-flow ratio, between Mach numbers of 0.9 and 1.2 (fig. 13(b)), also show no significant changes in lift.

Effect of Boundary-Layer Bypass Scoop and Fuselage Nose Configuration on Characteristics of Inlet Model

Pressure and force measurements with boundary-layer bypass scoop installed.- The losses in total pressure at the compressor-face station at Mach numbers above 1.0 were shown to be caused largely by shock and shock–boundary-layer interaction effects. It appeared, therefore, that the application of some method of boundary-layer control would result in pressure recovery gains. Removal of the boundary layer by means of the bypass scoop shown in figure 4 represents one such method.

With the scoop installed, the rate of mass flow to the compressor station was not appreciably different from the rate of mass flow through the inlet with the scoop removed $\left(\frac{m_i}{m_o} = 0.70\right)$. The mass-flow ratio based on the rate of mass flow through both the compressor station and the bypass scoop, however, varied from about 0.74 to 0.77 over the test Mach number range. Thus, the scoop flow varied from about $5\frac{1}{2}$ to $6\frac{1}{2}$ percent of the total inlet mass flow over the Mach number range.

Total-pressure recoveries at the compressor-face station with the scoop installed are compared in figure 14 with those obtained with the original inlet and with the maximum recovery available to the inlet as determined from the assumed shock formations ahead of the inlet. For the full range of test Mach number and angle of attack, the bypass scoop configuration produced recoveries greater than the original inlet. At a Mach number of 1.2, where boundary-layer–shock interaction effects became severe in the case of the original inlet, an increase in total-pressure recovery of $0.03H_o$ was obtained with the bypass scoop. For

the highest test Mach number of 1.41, the increase in recovery amounted to about $0.06H_o$ based on extrapolation of the original inlet data. The major part of the increases in recovery with the bypass scoop configuration is attributed to removal of the fuselage boundary layer ahead of the inlet.

Comparison of the recovery obtained with the scoop and the estimated maximum available shows that over the range of supersonic Mach number, the recovery at the compressor face with boundary-layer removal was within $0.05H_o$ of the maximum recovery possible with the assumed shock configurations. Losses in recovery of $0.03H_o$ to $0.04H_o$ are accountable throughout the Mach number range to local inlet and ducting losses. It is evident, therefore, that only a very small further gain in recovery would be possible with modifications to the present bypass scoop configuration. It is believed that additional gains in recovery through the test Mach number range or at higher Mach numbers can be obtained only through more efficient compression ahead of the inlet or by more efficient internal ducts.

In order to obtain the change in over-all performance due to installation of the boundary-layer bypass scoop, the changes in both pressure recovery and drag must be considered. If it is assumed that the original inlet will satisfy the air-flow requirements of a turbojet-engine capable of propelling an airplane with the original inlet configuration at a Mach number of 1.4, the increase in total-pressure recovery obtained with the bypass scoop configuration can be converted into an increase in net thrust, or a corresponding permissible increase in external drag. The increase in external drag necessary to offset exactly the increase in recovery has been calculated and added to the drag of the original inlet without a bypass scoop. The variation of this revised drag coefficient with Mach number is presented as the long-dash curve in the middle part of figure 14. It is noted that this drag is considerably greater than the measured external drag with the bypass scoop for all Mach numbers greater than about 1.08. Actually, only a small increment in external drag was incurred in discharging the boundary-layer flow from the model.

The net gain for the scoop configuration can be more clearly shown by relating the increase in net thrust, due to increases in total-pressure recovery, to the increases in external drag. This effectiveness parameter $\Delta F_N - \Delta D$ is shown in the lower part of figure 14 as a percentage of the net thrust for 100-percent pressure recovery, which was obtained from an analysis and correlation of current jet-engine performance data. This relation shows that at all Mach numbers above about 1.08 a gain in performance would be obtained with the bypass scoop configuration. At a Mach number of 1.41 the gain in thrust minus drag would be about 7.8 percent of the net thrust for 100-percent pressure recovery.

Pressure and force measurements with conical fuselage nose and with blunt nose having roughness installed at leading edge.- Installation of the conical fuselage nose caused no significant changes in the boundary-layer–shock phenomena at the inlet and, within the accuracy of measurement, no changes in the average total pressures at the compressor face for the present test range of Mach and Reynolds numbers although the fuselage nose shock was attached at Mach numbers above about 1.04. The conical nose also caused no appreciable changes in the external drag for the range of Mach number through which it was tested. This was believed due to the relatively small changes in shock loss with shock form at these Mach numbers.

Installation of roughness on the blunt-nose fuselage did not cause significant changes in either the total-pressure ratio at the compressor-face station or in the external drag.

SUMMARY OF RESULTS

An investigation has been made in the Langley transonic blowdown tunnel at Mach numbers from 0.80 to 1.41 to determine the increments in lift and drag due to installation of a triangular-shaped air inlet in the root of a 45° sweptback wing and to study the internal flow characteristics of the inlet. The test ranges of angle of attack and mass-flow ratio varied from -2.0° to 8.2° and 0.34 to 0.77, respectively. The more important results are summarized as follows:

1. Total-pressure recoveries at the assumed engine-face station increased with increases in mass-flow ratio at all angles of attack and Mach numbers tested. The fuselage boundary layer that entered the inlet and its interaction with the shock just ahead of the inlet caused a major part of the measured total-pressure losses.

2. At a test mass-flow ratio of about 0.70 a total-pressure recovery of 90 percent or greater was obtained without a bypass scoop for all test angles of attack up to a Mach number of 1.20.

3. Installation of a bypass scoop extended the Mach number range for a pressure recovery of 90 percent or greater to 1.36. The drag increment due to the bypass was small and a maximum estimated gain in thrust minus drag of 7.8 percent of the 100-percent pressure-recovery thrust was obtained at a Mach number of 1.41.

4. The drag increment due to the inlet was small throughout the test ranges of mass-flow ratio and Mach number for angles of attack up to about 3°. At higher angles of attack the drag increment became appreciable in the Mach number range around 1.1, and then decreased with further increases in Mach number.

5. The increment in lift due to the inlet was positive except for the highest angles of attack at the highest Mach numbers. In general, the lift increment was approximately in proportion to the increase in wing area caused by the inlet installation.

Langley Aeronautical Laboratory,
National Advisory Committee for Aeronautics,
Langley Field, Va.

APPENDIX

METHOD USED IN DETERMINING EXTERNAL-DRAG AND LIFT INCREMENTS OF PRESENT WING-ROOT AIR INLET

The following discussion will show the method which was used in determining the external-drag and lift increments due to installation of the present wing-root air inlet on the basic wing-body configuration.

> The external-drag increment of an air inlet is defined as the difference between the external drag of the basic streamline body and that of the same body when modified only by installation of the air inlet.

The application of this definition to the actual inlet configuration is not direct, inasmuch as the external-drag increment of a body that is admitting and discharging air cannot be measured directly, but must be obtained by computation. The basic or reference drag of the configuration is taken to be that of the basic wing-body combination. The body to be compared with the reference body is one having an air inlet and admitting air but, inasmuch as the shape must otherwise be the same as that of the basic body, can have no air exit. If it were possible to measure the total drag of such a configuration, the external drag would be equal to the measured total drag diminished by the net rate of change of momentum of the air admitted but not discharged; that is, the external drag would be equal to the measured drag minus mV_O. This is so because the mass flow per unit time m admitted to the body originally had a velocity V_O relative to the body and is finally brought to rest within the body.

The problem then resolves itself into the determination of the total drag of a body of basically the same shape as the reference body but fitted with an air inlet and admitting air. The drag of this body must be obtained indirectly from measurements of the total drag of a body that is both admitting and discharging air. Let the body with the air inlet and exit be represented by the body shown cross-hatched in figure 15. The total force in the stream direction measured on the body is equal to the surface integral of the components of pressure and momentum transfer across any closed boundary surounding the body, or

$$D_{measured} = \int_A (p \cos \theta + \rho V_N \vec{V} \cos \theta_1) dA \qquad (1)$$

where

p pressure at boundary

θ angle between an inwardly directed normal to an element of boundary and free-stream direction

ρ density at any point on boundary

V_N component of velocity normal to the boundary, positive for entering flow, negative for flow exiting the boundary

$\vec{V}$ vector velocity at any point on boundary

θ_1 angle between $\vec{V}$ and the free-stream direction

The contribution to this integral of the jet-exit velocity is equal to

$$-\int_{A_x} \rho V_x^2 dA$$

The minus sign results from the fact that the flow is exiting the boundary.

Experimental data (refs. 3, 4, and 5) indicate that large variations of the flow into an air inlet have a negligible effect on the pressure distribution over the body in regions sufficiently far downstream from the inlet plane. Consequently, it appears reasonable to assume that, if the inlet body on which the measurements are made was faired at the rearward portion in the same manner as the basic streamline body, the pressure distribution over this portion of the inlet and basic bodies would be the same provided the inlet does not cause separation.

Investigations of exits have shown (refs. 6 and 7) that the effect of the exit flow on the pressures over the body is confined to a limited region in the vicinity of the exit. In general, therefore, there should be a region of considerable extent over which neither the air inlet nor exit will have any effect on the pressure distribution. If the contour A, figure 15, is drawn in the manner indicated, with the points B and C in the region unaffected by the presence of either inlet or exit, the total drag of the inlet body which admits but does not discharge air, and which is faired in the region of the exit in the same manner as the basic body can be found by the method indicated in figure 15. This process may be described more in detail as follows:

To the integral around path A, after the effect of the jet-exit velocity is removed, is added the corresponding integral around path T, where the two paths coincide over the region DE. A correction is applied to the integral around path A to allow for the fact that the pressure distribution in the region BDEC would be different with a continuously faired tail cone from the values actually existing over that portion of the body with the exit in operation. The pressure over the region DE of the tail cone is taken to be the same as that in the corresponding region of contour A in order that the contribution to the total closed path integral A + T of the internal line DE shall be zero. The final desired expression for the external-drag increment of the air inlet is then

$$\Delta D_{ext} = D_{m_i} + \int_{A_x} \rho V_x^2 dA + \int_T p \, dT + \int_{BDEC} \Delta p \, dA - mV_o - D_{m_b} \qquad (2)$$

where the integral

$$\int_{A_x} \rho V_x^2 dA = \overline{mV}_x$$

is obtained from the measurements in the jet of the inlet model, the integral

$$\int_T p \, dT = (\overline{p}_x - p_o)A_x - (\overline{p}_T - p_o)A_T$$

is obtained from pressure-distribution measurements on the tail cone of the basic model and from static-pressure measurements in the jet exit (where the projected area of the tail cone A_T is equal to A_x), and the integral

$$\int_{BDEC} \Delta p \, dA = \left(\overline{p}_{\substack{\text{rear} \\ \text{inlet model}}} - \overline{p}_{\substack{\text{rear} \\ \text{basic model}}}\right) A_{BDEC}$$

is obtained from comparison of the external pressure-distribution measurements on the rear end of the air-inlet model fuselage with the jet in operation with corresponding pressures on the basic-model fuselage.

Equation (2) can be rewritten in the following form by summing the terms after integration:

$$\Delta D_{ext} = D_{mi} - m(V_o - \overline{V}_x) + (\overline{p}_x - p_o)A_x - (\overline{p}_T - p_o)A_T +$$

$$\left(\overline{p}_{\substack{\text{rear} \\ \text{inlet model}}} - \overline{p}_{\substack{\text{rear} \\ \text{basic model}}}\right)A_{BDEC} - D_{mb} \qquad (3)$$

The increment in drag as defined by equation (3) is the same as the drag increment generally used which is defined as

$$\Delta D_{ext} = D_{mi} - \left[m(V_o - \overline{V}_x) - (\overline{p}_x - p_o)A_x\right] - \left[D_{mb} + (\overline{p}_B - p_o)A_x\right] \qquad (4)$$

except that in equation (4) the term $\left(\overline{p}_{\substack{\text{rear} \\ \text{inlet model}}} - \overline{p}_{\substack{\text{rear} \\ \text{basic model}}}\right)A_{BDEC}$ has been neglected. In equation (4), D_{mb} is equal to the measured drag of the basic model having the fuselage afterbody cut off at a position corresponding to the exit location on the inlet model ($A_B = A_x = A_T$). The range of values of the correction $\left(\overline{p}_{\substack{\text{rear} \\ \text{inlet model}}} - \overline{p}_{\substack{\text{rear} \\ \text{basic model}}}\right)A_{BDEC}$ for the range of test variables is indicated in the following table; a range of values of $(\overline{p}_T - p_o)A_T$ is also presented:

M_o	m_i/m_o	$\frac{\left(\bar{p}_{rear\ inlet\ model} - \bar{p}_{rear\ basic\ model}\right)A_{BDEC}}{q_oS}$	$\frac{(\bar{p}_T - p_o)A_T}{q_oS}$
0.85	0.34 .70	0.0008 .0008	0.0015 .0031
1.02	.39 .71	.0013 .0013	.0018 .0043
1.25	.39 .75	.0008 .0008	.0019 .0023

Equation (3) applies for the external-drag increment of an air inlet for the 0° angle-of-attack case. For angles other than 0°, the relation becomes

$$\Delta D_{ext} = D_{mi} + \left[m\bar{V}_x + (\bar{p}_x - p_o)A_x - (\bar{p}_T - p_o)A_T + \left(\bar{p}_{rear\ inlet\ model} - \bar{p}_{rear\ basic\ model}\right)A_{BDEC} \right] \cos \alpha - mV_o - D_{mb} \quad (5)$$

The increment in lift due to the inlet can be similarly determined by

$$\Delta L_{ext} = L_{mi} + \left[m\bar{V}_x + (\bar{p}_x - p_o)A_x - (\bar{p}_T - p_o)A_T + \left(\bar{p}_{rear\ inlet\ model} - \bar{p}_{rear\ basic\ model}\right)A_{BDEC} \right] \sin \alpha - L_{mb} \quad (6)$$

REFERENCES

1. Keith, Arvid L., Jr., and Schiff, Jack: Low-Speed Wind-Tunnel Investigation of a Triangular Sweptback Air Inlet in the Root of a 45° Sweptback Wing. NACA RM L50I01, 1950.

2. Wright, Ray H., and Ward, Vernon G.: NACA Transonic Wind-Tunnel Test Sections. NACA RM L8J06, 1948.

3. Nichols, Mark R., and Keith, Arvid L., Jr.: Investigation of a Systematic Group of NACA 1-Series Cowlings With and Without Spinners. NACA Rep. 950, 1949. (Supersedes NACA RM L8A15.)

4. Pendley, Robert E., and Smith, Norman F.: An Investigation of the Characteristics of Three NACA 1-Series Nose Inlets at Subcritical and Supercritical Mach Numbers. NACA RM L8L06, 1949.

5. Pendley, Robert E., and Robinson, Harold L.: An Investigation of Several NACA 1-Series Nose Inlets With and Without Protruding Central Bodies at High-Subsonic Mach Numbers and at a Mach Number of 1.2. NACA RM L9L23a, 1950.

6. Becker, John V.: Wind-Tunnel Investigation of Air Inlet and Outlet Openings on a Streamline Body. NACA Rep. 1038, 1951. (Supersedes NACA ACR, Nov. 1940.)

7. Love, Eugene S.: Aerodynamic Investigation of a Parabolic Body of Revolution at Mach Number of 1.92 and Some Effects of an Annular Jet Exhausting From the Base. NACA RM L9K09, 1950.

TABLE I - DIMENSIONS OF BASIC AND DUCTED WING

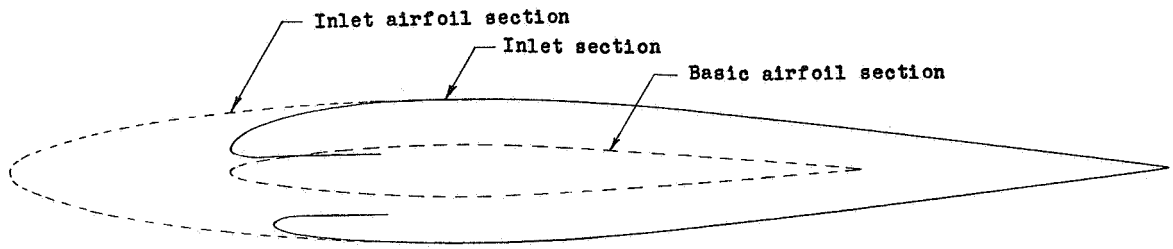

Semispan wing station (in.)	Basic wing			Ducted wing				
	c (in.)	t (percent c)	c/4 sweep	Total c (in.) (a)	t (percent total c)	c/4 sweep	Inlet c (in.) (b)	t (percent inlet c)
0	5.587	8	45°					
[c] 1.347	5.250	8	45°	10.500	13.00	55°	8.331	16.38
1.625	5.180	8	45°	9.540	12.30	55°	7.712	15.22
2.062	5.071	8	45°	8.019	11.20	55°	6.732	13.34
2.500	4.962	8	45°	6.515	10.04	55°	5.765	11.35
3.000	4.837	8	45°	5.108	8.80	55°	4.893	9.19
[d] 3.090	4.815	8	45°	4.984	8.55	55°	4.830	8.82
3.250	4.774	8	45°	4.831	8.10	55°	4.775	8.19
3.284	4.766	8	45°	4.801	8.00	55°	4.766	8.06
3.347	4.750	8	45°	4.750	8.00	45°	4.750	8.00
4.500	4.462	8	45°	4.462	8.00	45°	4.462	8.00
9.000	3.337	8	45°	3.337	8.00	45°	3.337	8.00

(a) Chord before installation of inlet.
(b) Leading edge of ducted wing coincident with leading edge of basic wing.
(c) Juncture of fuselage with leading edge at fuselage station 5.00.
(d) Outboard corner of inlet.

TABLE II DIMENSIONS OF WING-ROOT INLET CONFIGURATION

[All dimensions in inches]

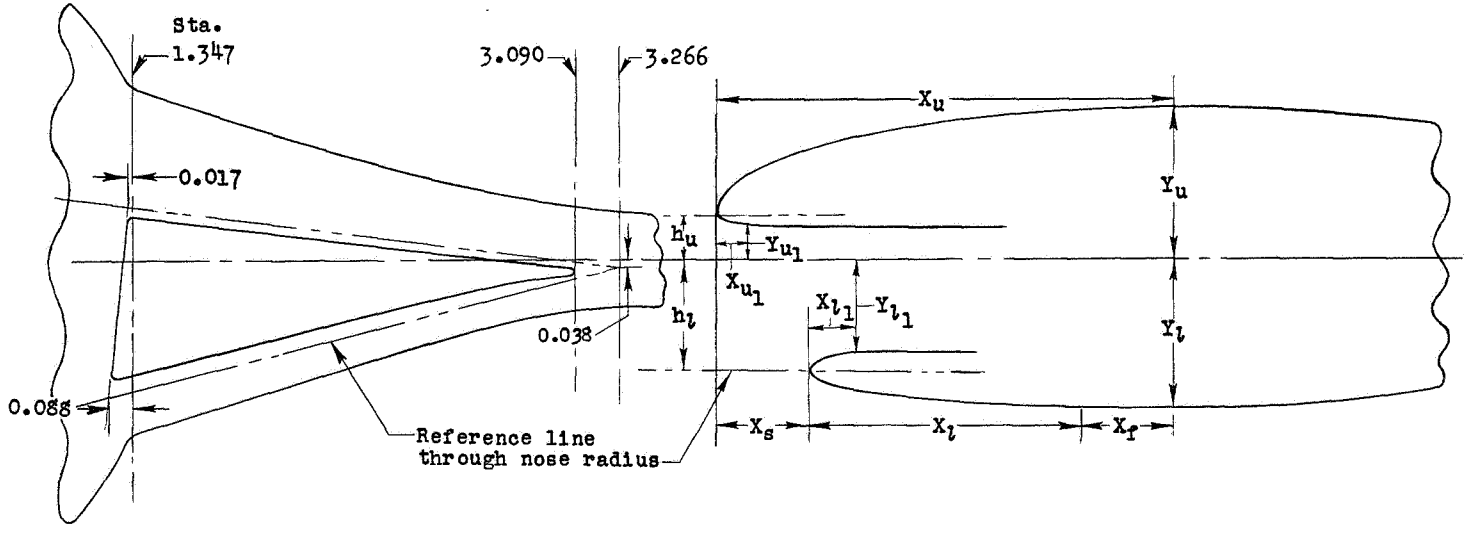

Wing station	External surfaces (a)								Internal surfaces (a)			
	h_u	X_u	Y_u	X_s	h_l	X_l	X_f (b)	Y_l	X_{u_1}	Y_{u_1}	X_{l_1}	Y_{l_1}
1.347	0.213	1.821	0.682	0.385	0.500	1.436	0	0.682	0.125	0.176	0.187	0.422
1.625	.177	1.797	.587	.352	.433	1.445	0	.587	.125	.140	.187	.358
2.062	.120	1.760	.451	.300	.327	1.241	.219	.451	.125	.082	.187	.257
2.500	.063	1.726	.327	.248	.222	1.041	.437	.327	.125	.025	.187	.157
3.000	-.003	1.727	.225	.188	.101	.852	.687	.225	.062	-.028	.187	.057

(a) External and internal nose shapes determined from elliptical ordinates.

(b) Flat on lower surface.

(a) Basic model (shown with pointed nose), three-quarter-front view from above.

Figure 1.- Photographs of the basic and inlet models.

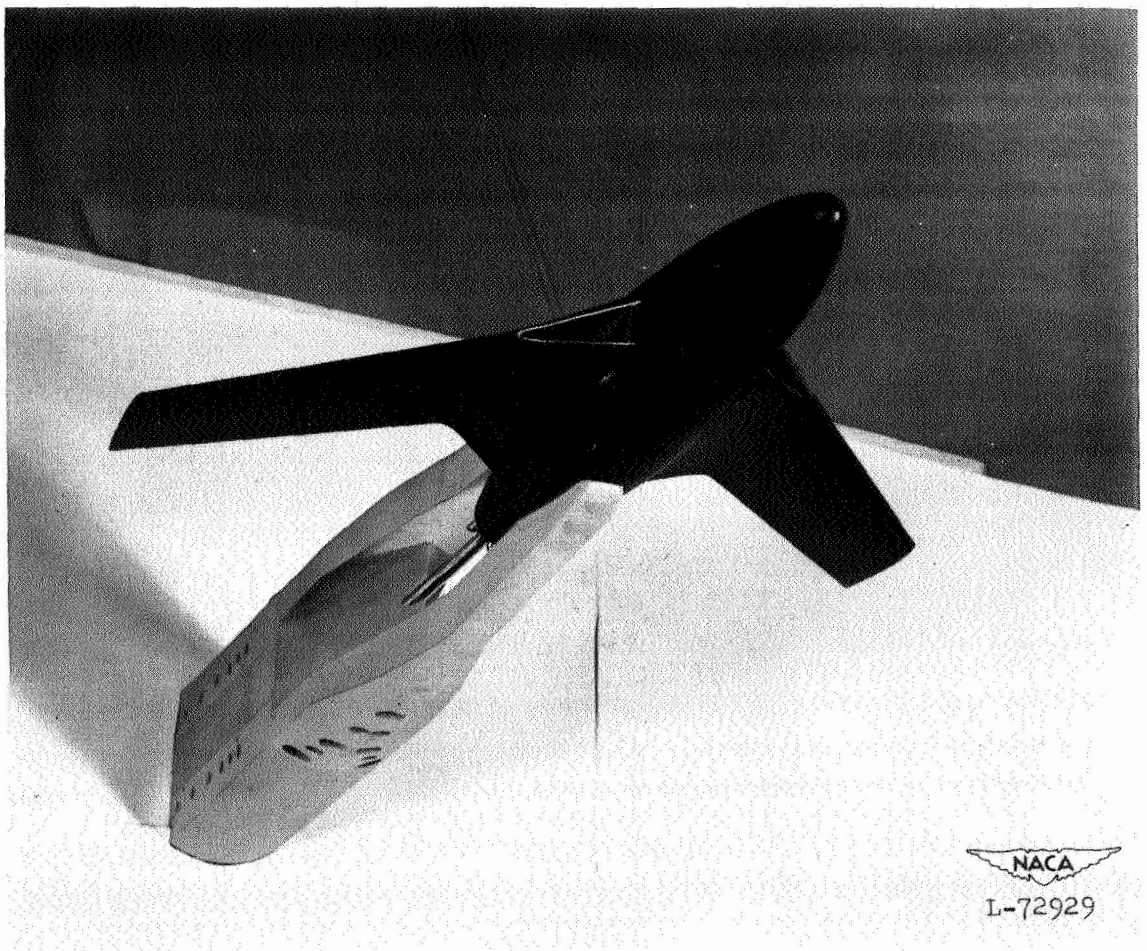

(b) Inlet model with boundary-layer bypass scoop, three-quarter-front view from below.

Figure 1.- Continued.

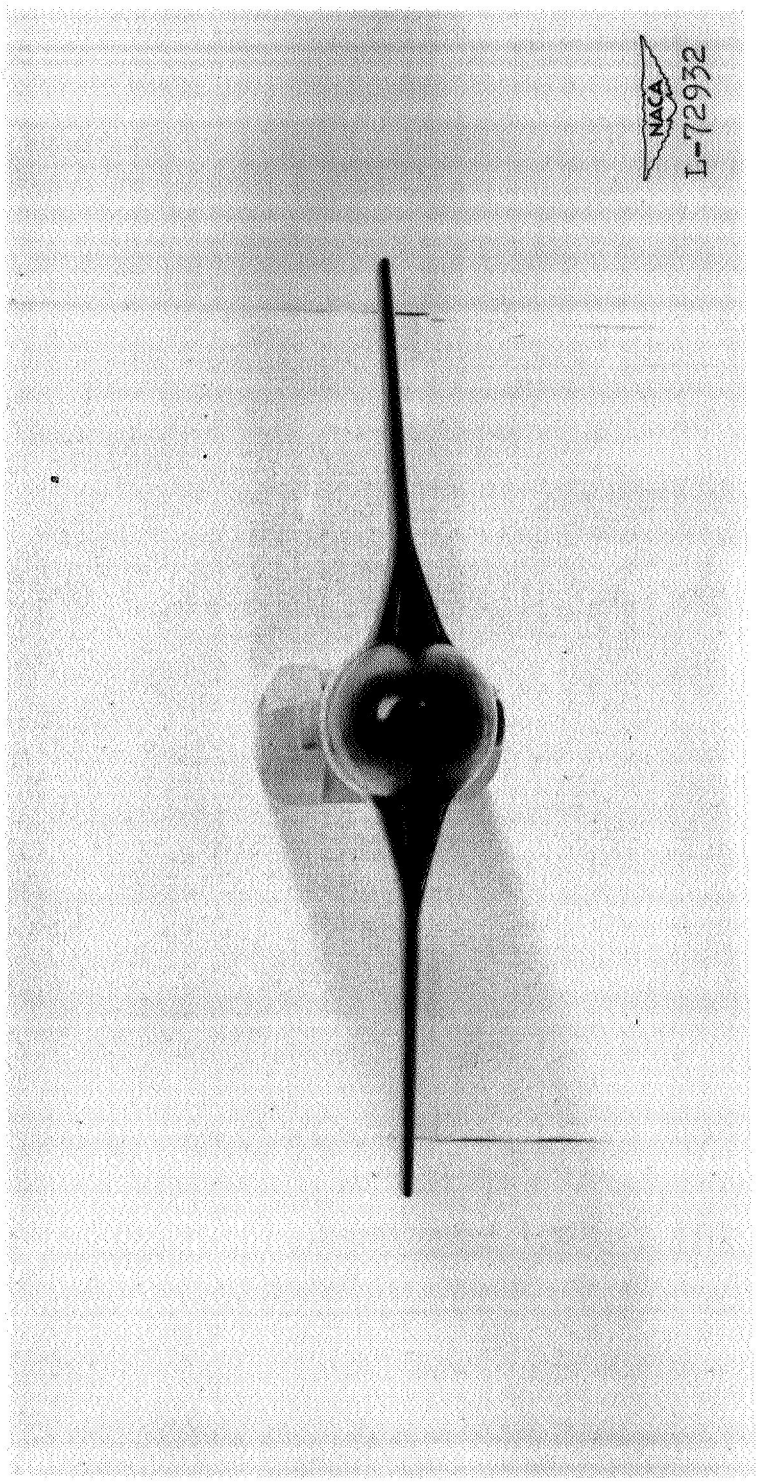

(c) Inlet model, front view.

Figure 1.- Concluded.

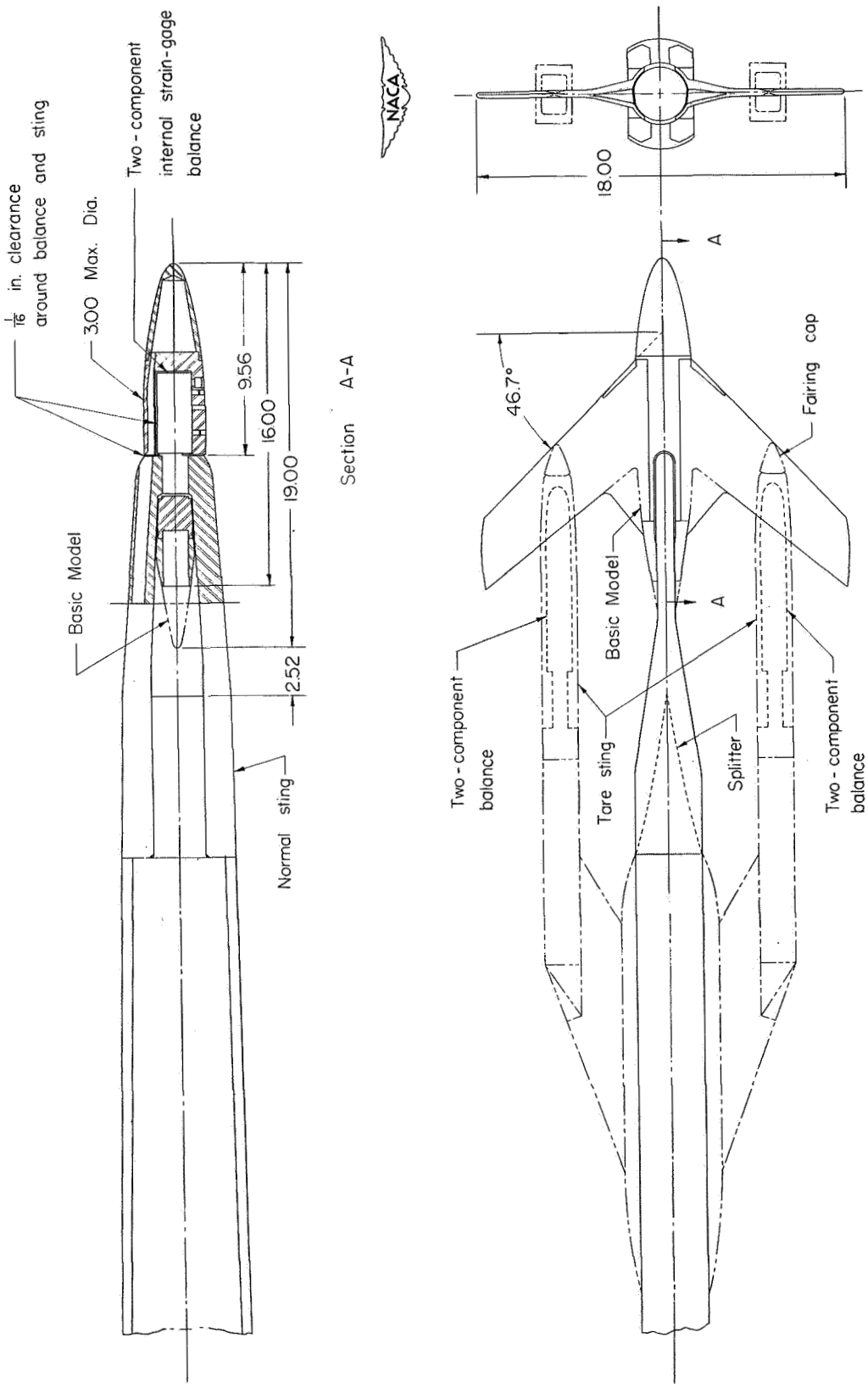

Figure 2.- General arrangement of models and model supports. All dimensions are in inches.

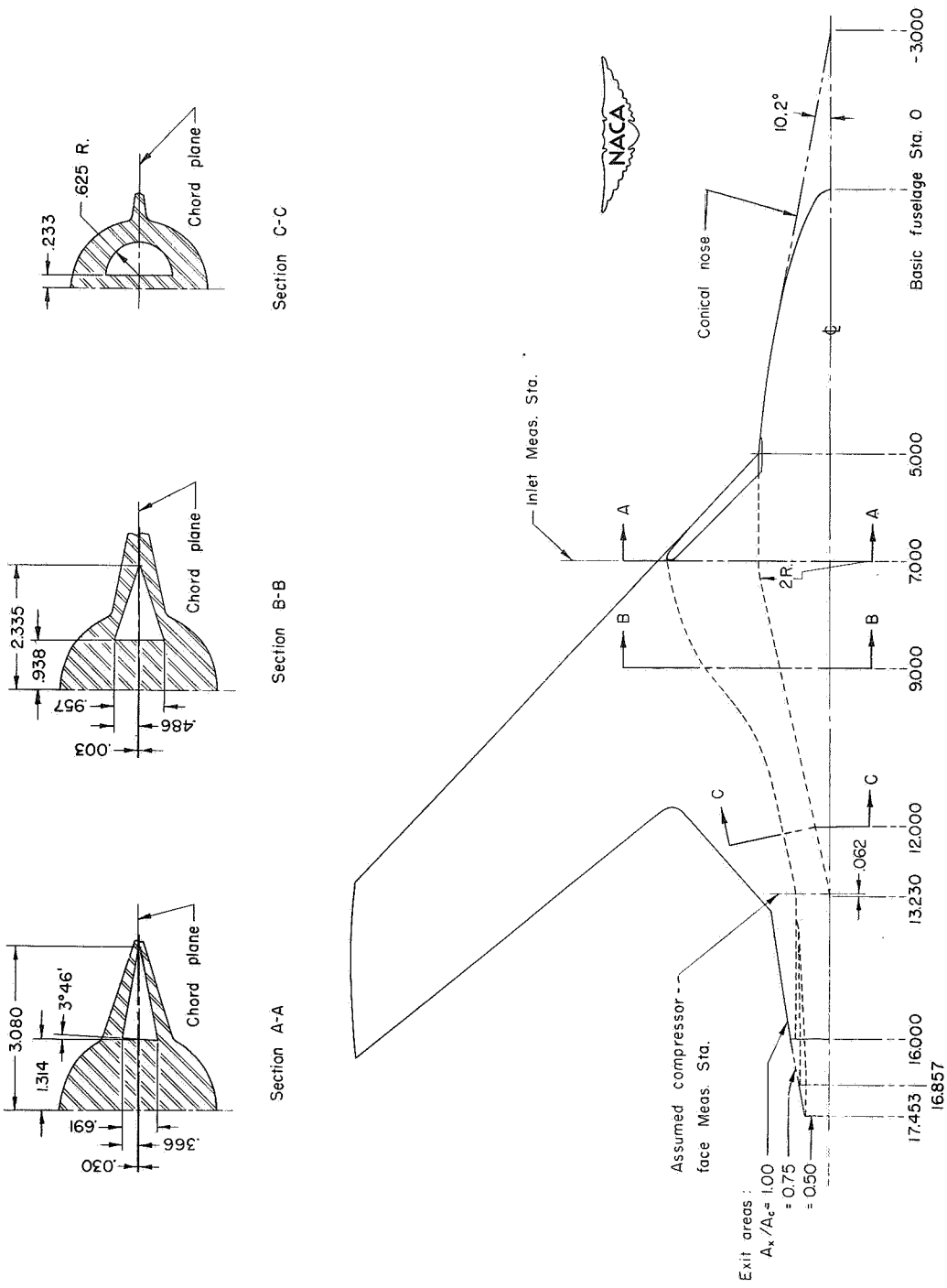

Figure 3.- Plan view of inlet model showing details of internal ducting and exit configuration. All dimensions are in inches.

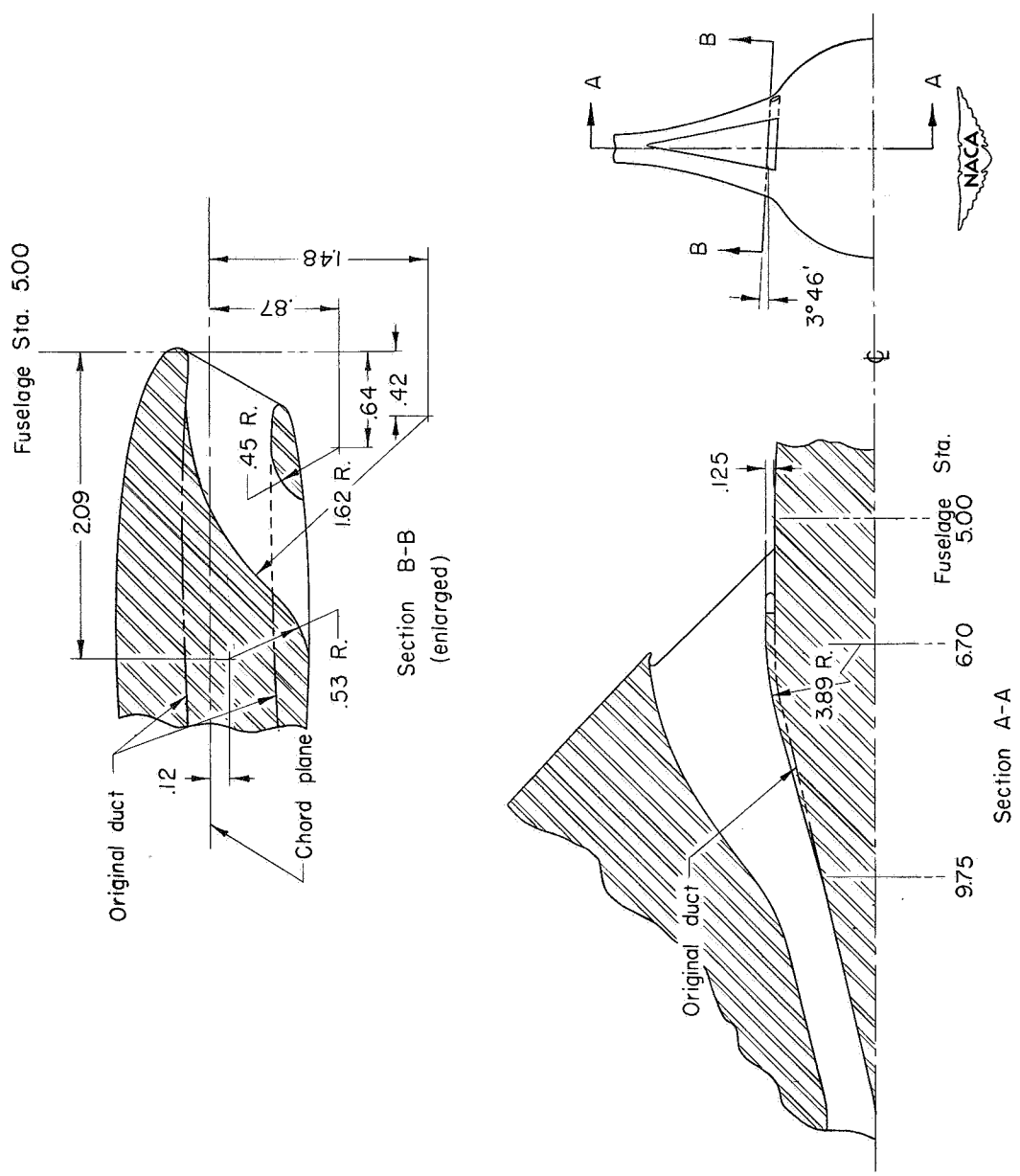

Figure 4.- Details of boundary-layer bypass scoop. All dimensions are in inches.

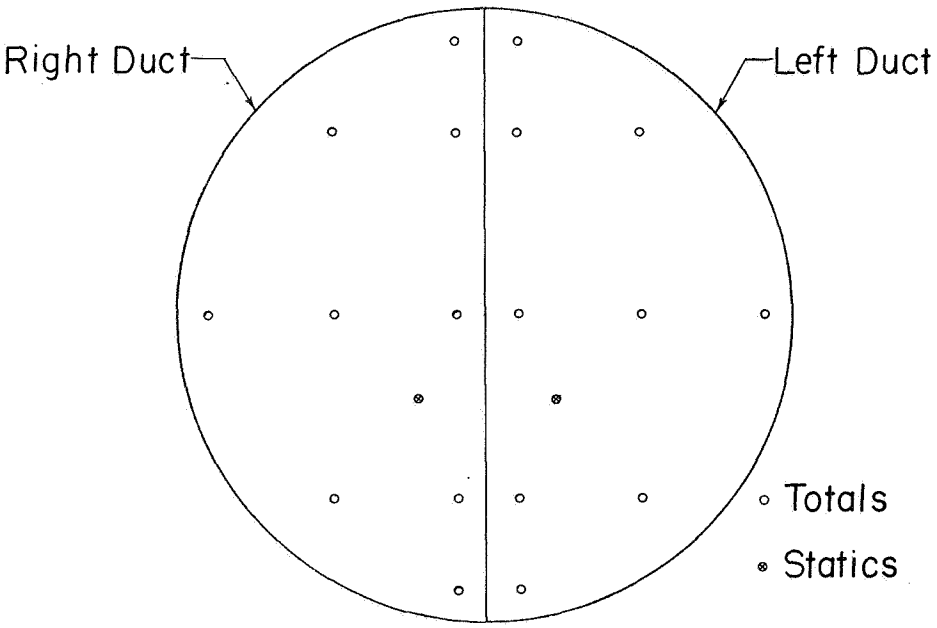

Tube distribution at the compressor-face measuring station

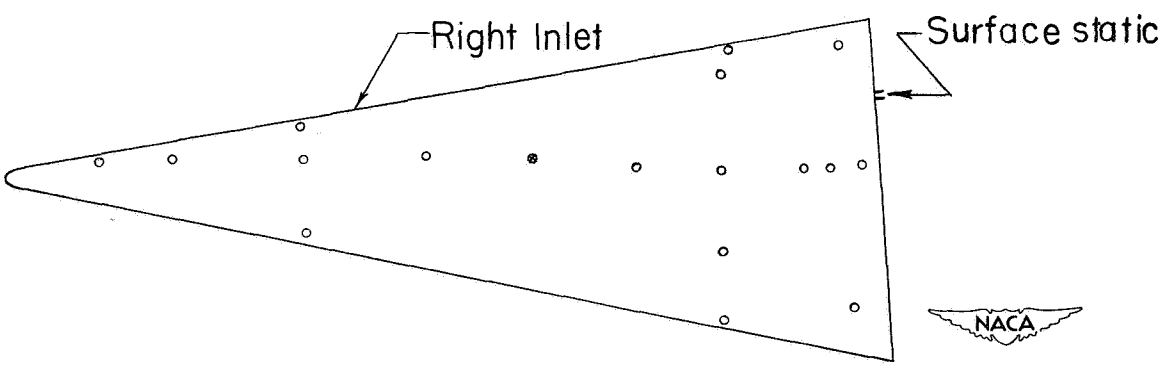

Tube distribution at the inlet measuring station

Figure 5.- Total- and static-pressure tube instrumentation at the inlet and compressor-face measuring station; viewed downstream.

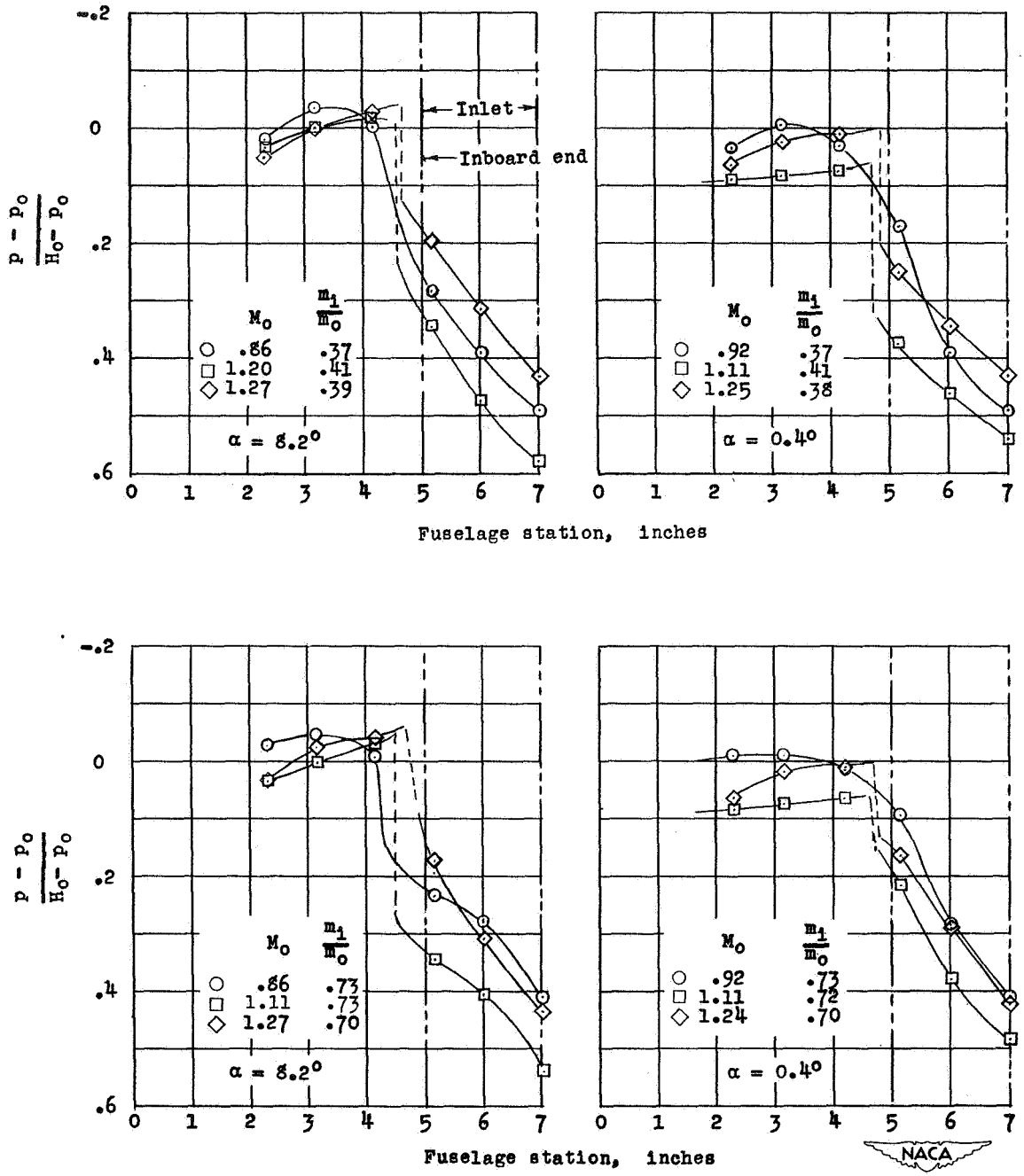

Figure 6.- Surface pressure distributions over nose of inlet model along horizontal center line.

Figure 7.- Contours of impact-pressure ratio at the inlet measuring station.

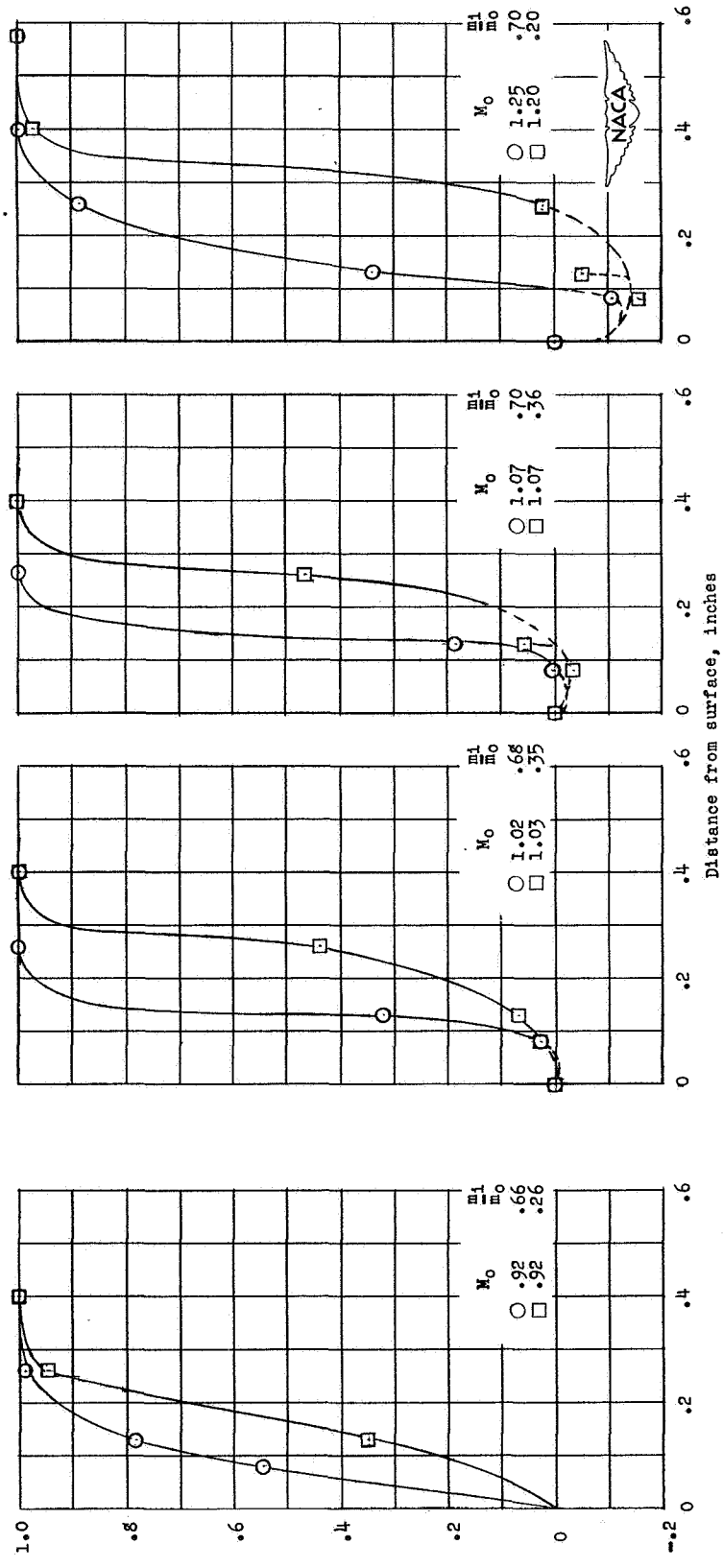

Figure 8.- Velocity distributions in the fuselage boundary layer at the inlet measuring station. $\alpha = 0.4^{\circ}$.

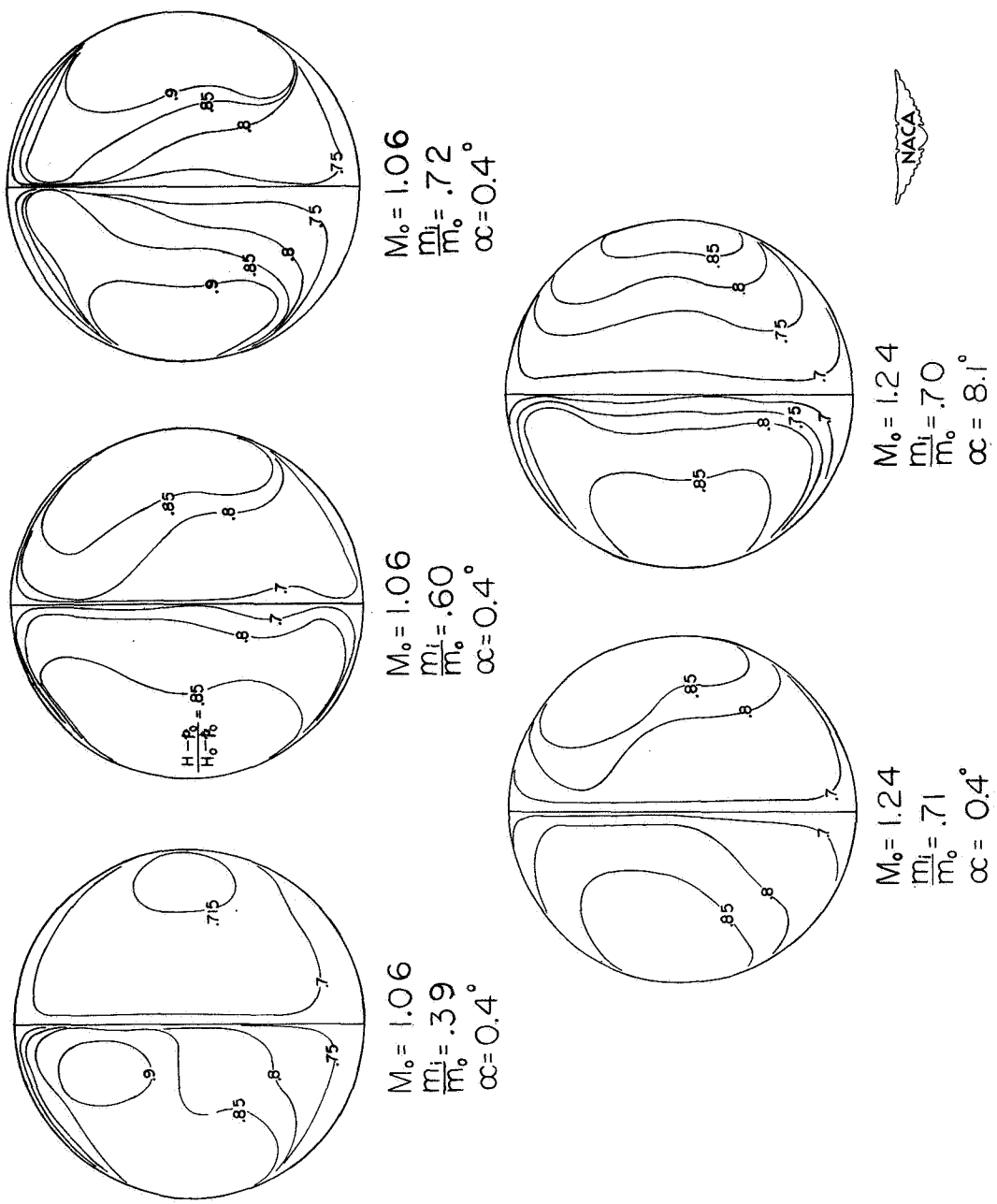

Figure 9.- Contours of impact-pressure ratio at compressor-face measuring station.

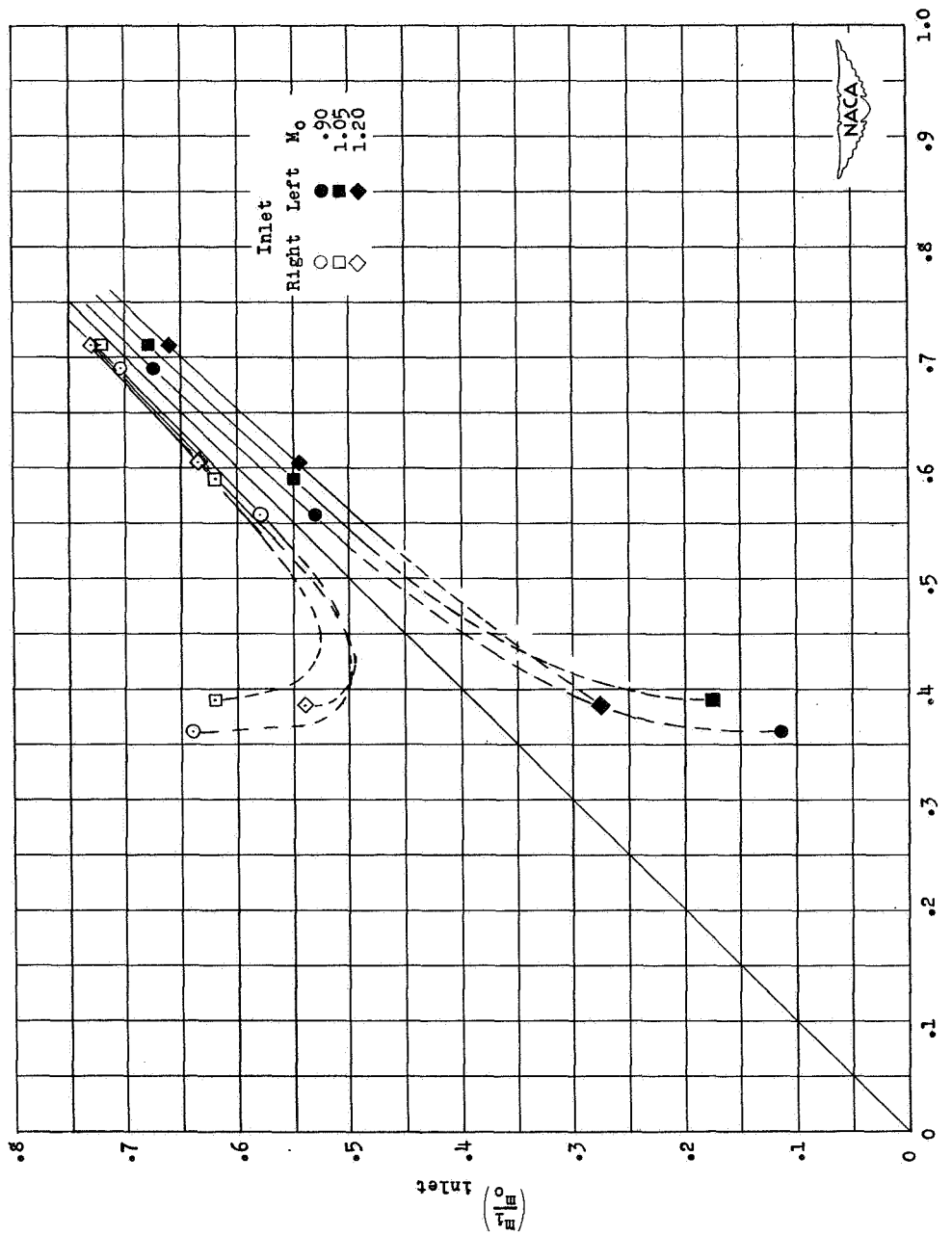

Figure 10.- Variation of mass-flow ratio through each inlet with system mass-flow ratio for several test Mach numbers at $\alpha = 0.4^{\circ}$.

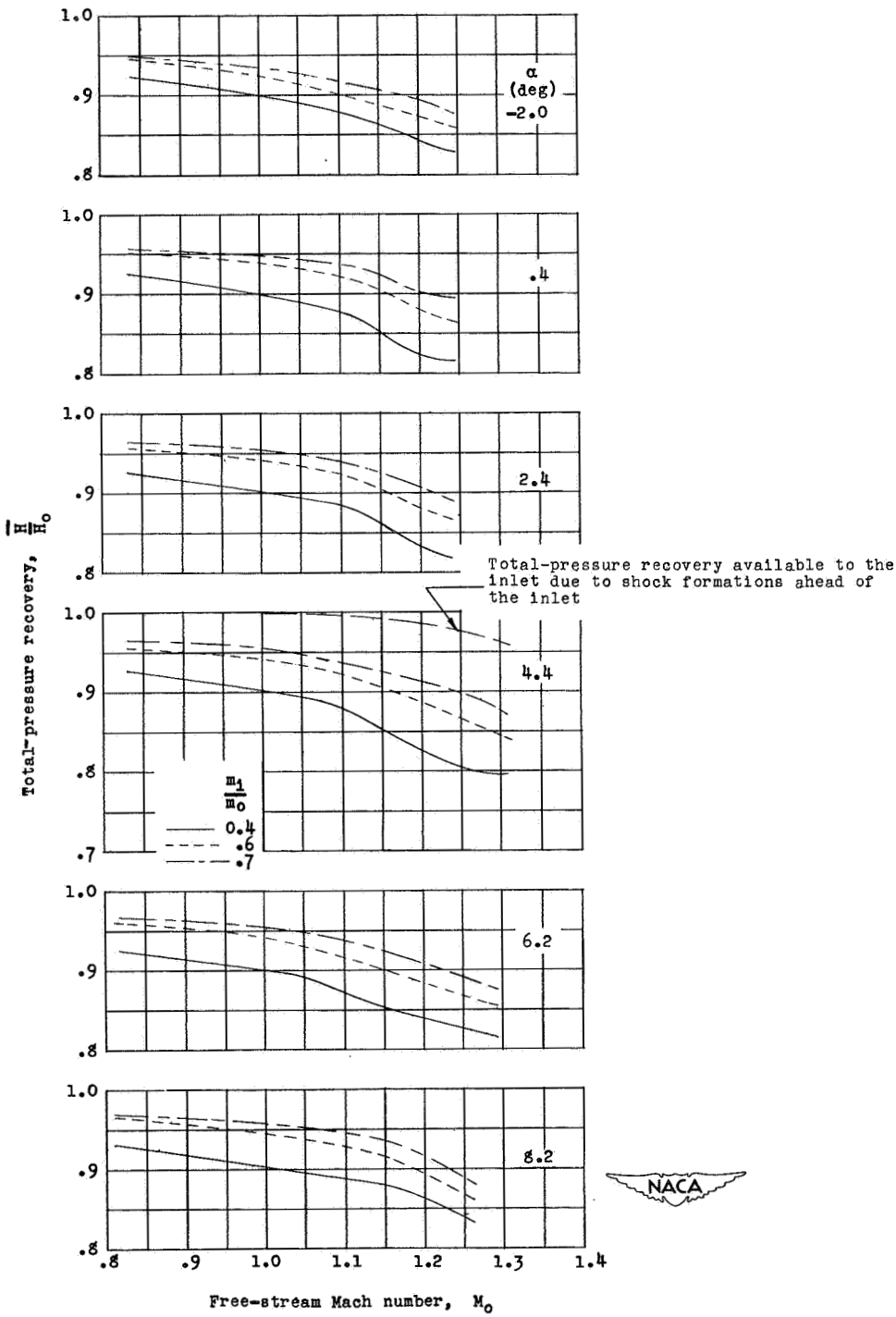

(a) Effect of Mach number.

Figure 11.- Effects of variations in Mach number, angle of attack, and mass-flow ratio on average integrated total-pressure ratio at compressor-face measuring station.

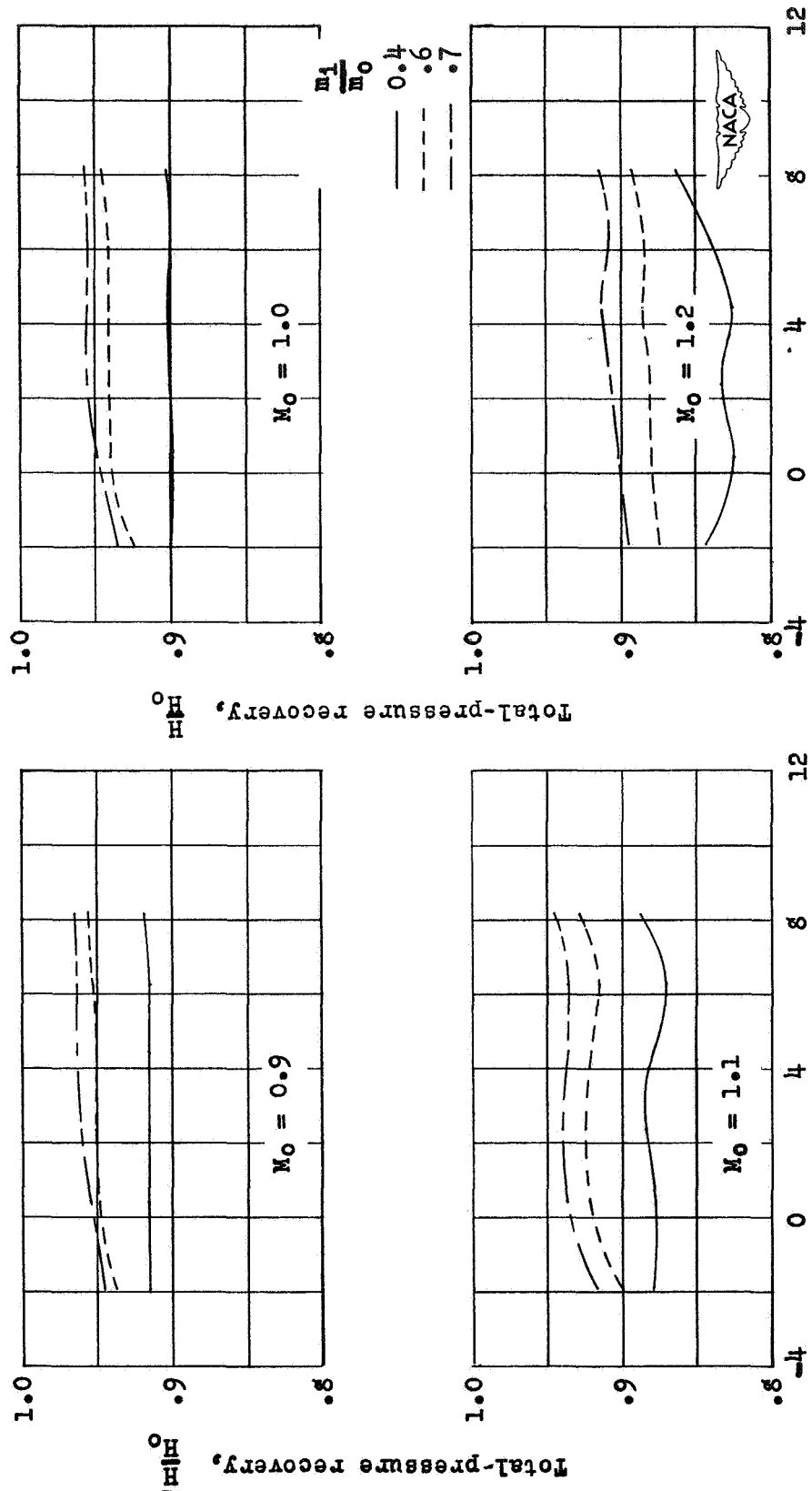

(b) Effect of angle of attack.

Figure 11.- Continued.

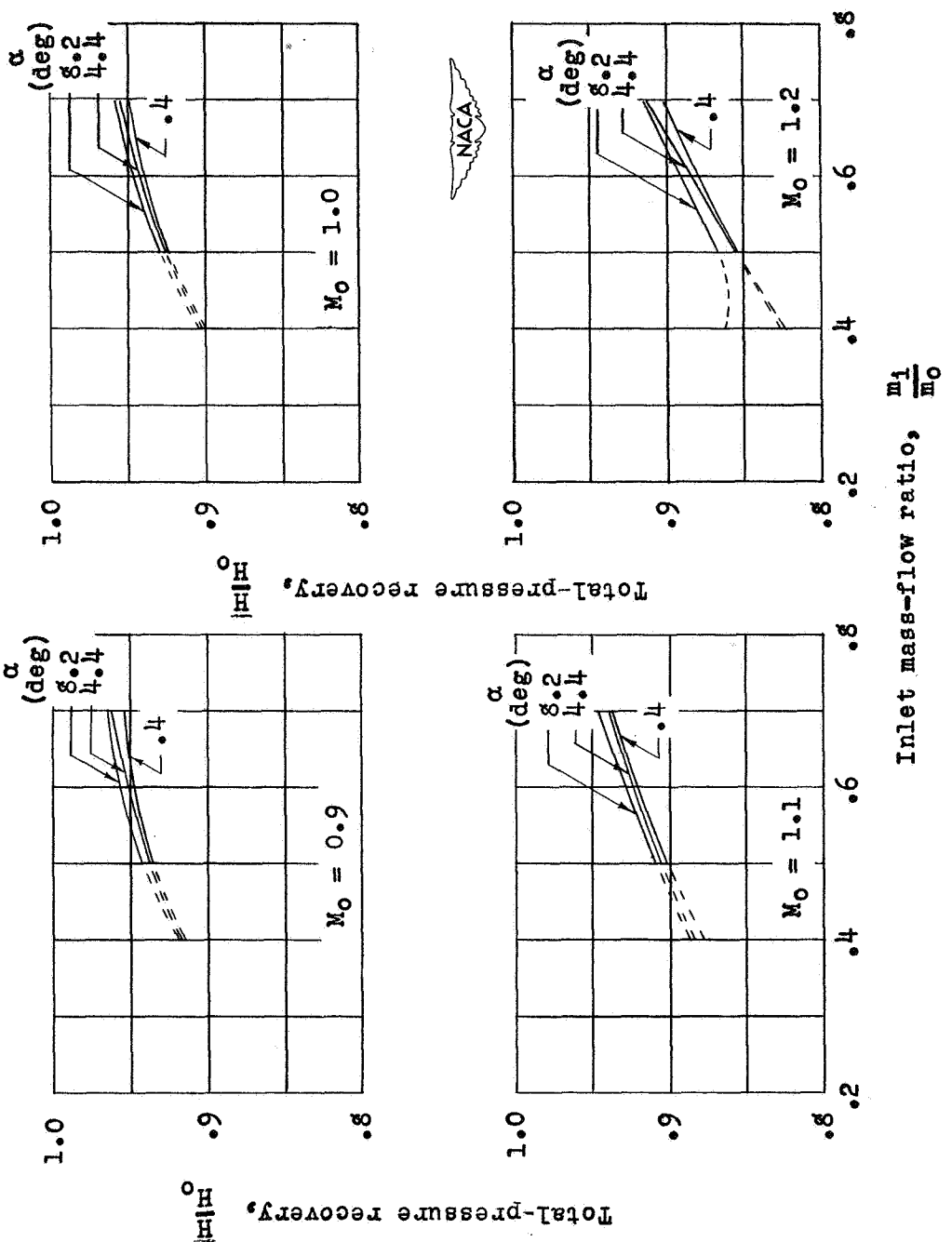

(c) Effect of mass-flow ratio.

Figure 11.- Concluded.

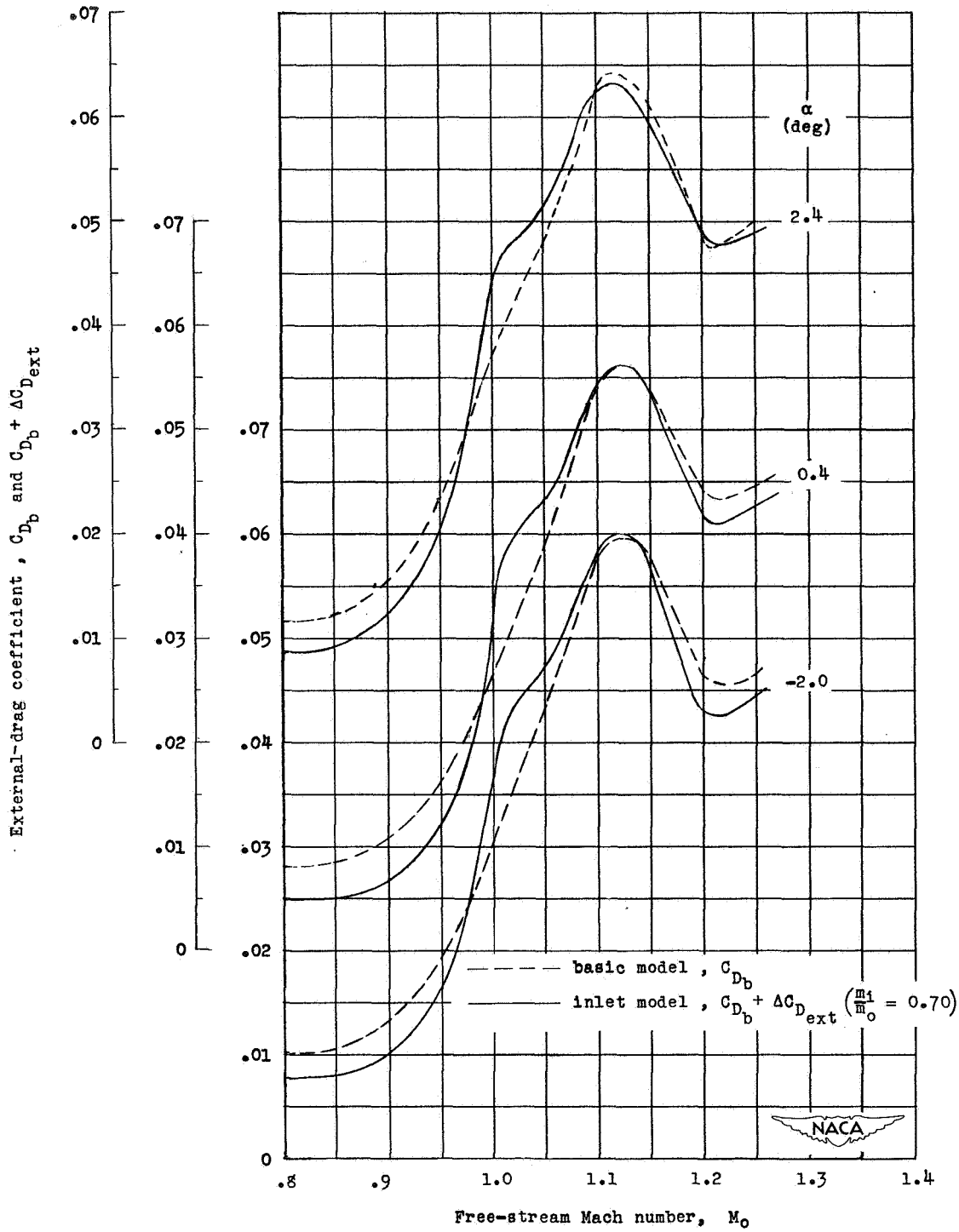

(a) Effect of Mach number. $\alpha = -2.0^\circ$, 0.4°, and 2.4°.

Figure 12.- Effects of variations in Mach number, angle of attack, and mass-flow ratio on the external-drag coefficient.

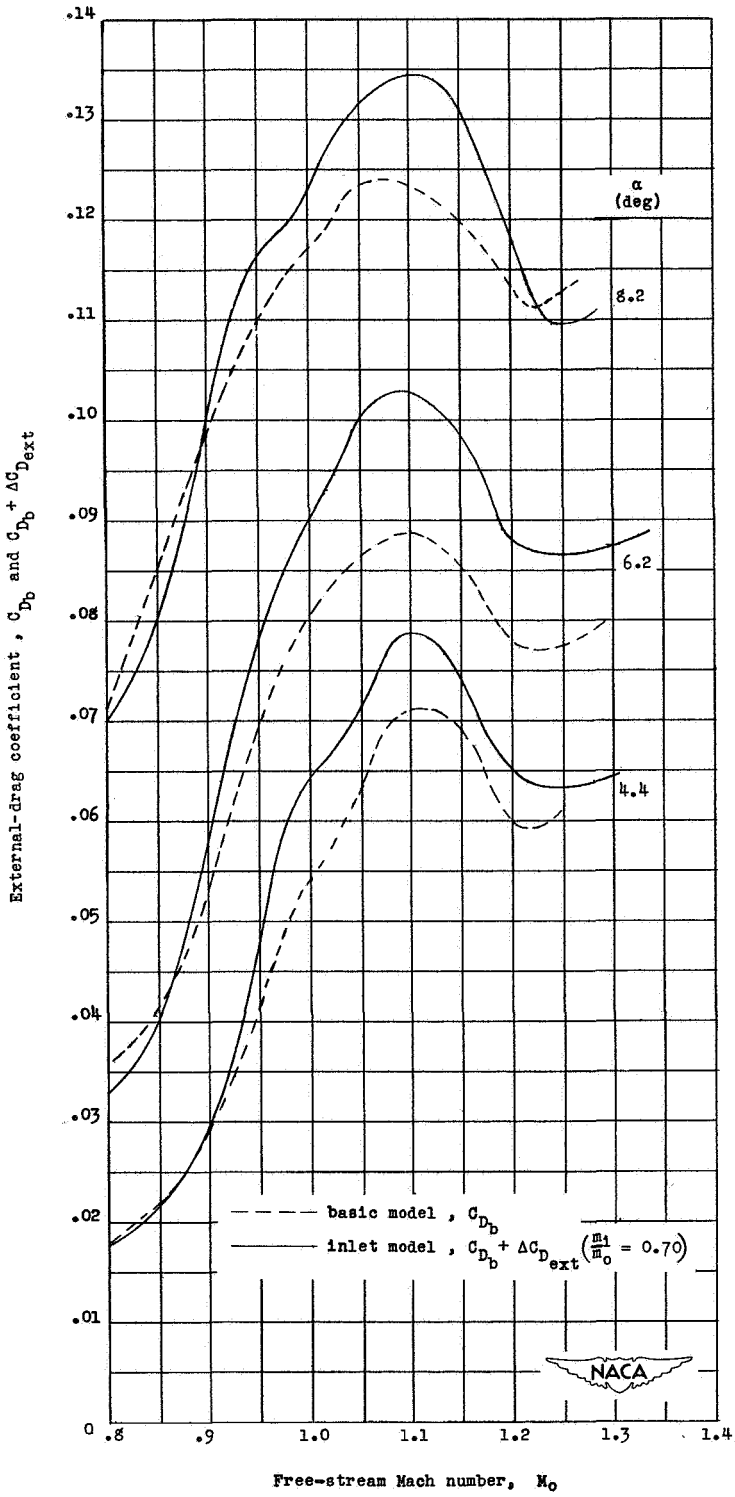

(b) Effect of Mach number. $\alpha = 4.4^{\circ}$, 6.2°, and 8.2°.

Figure 12.- Continued.

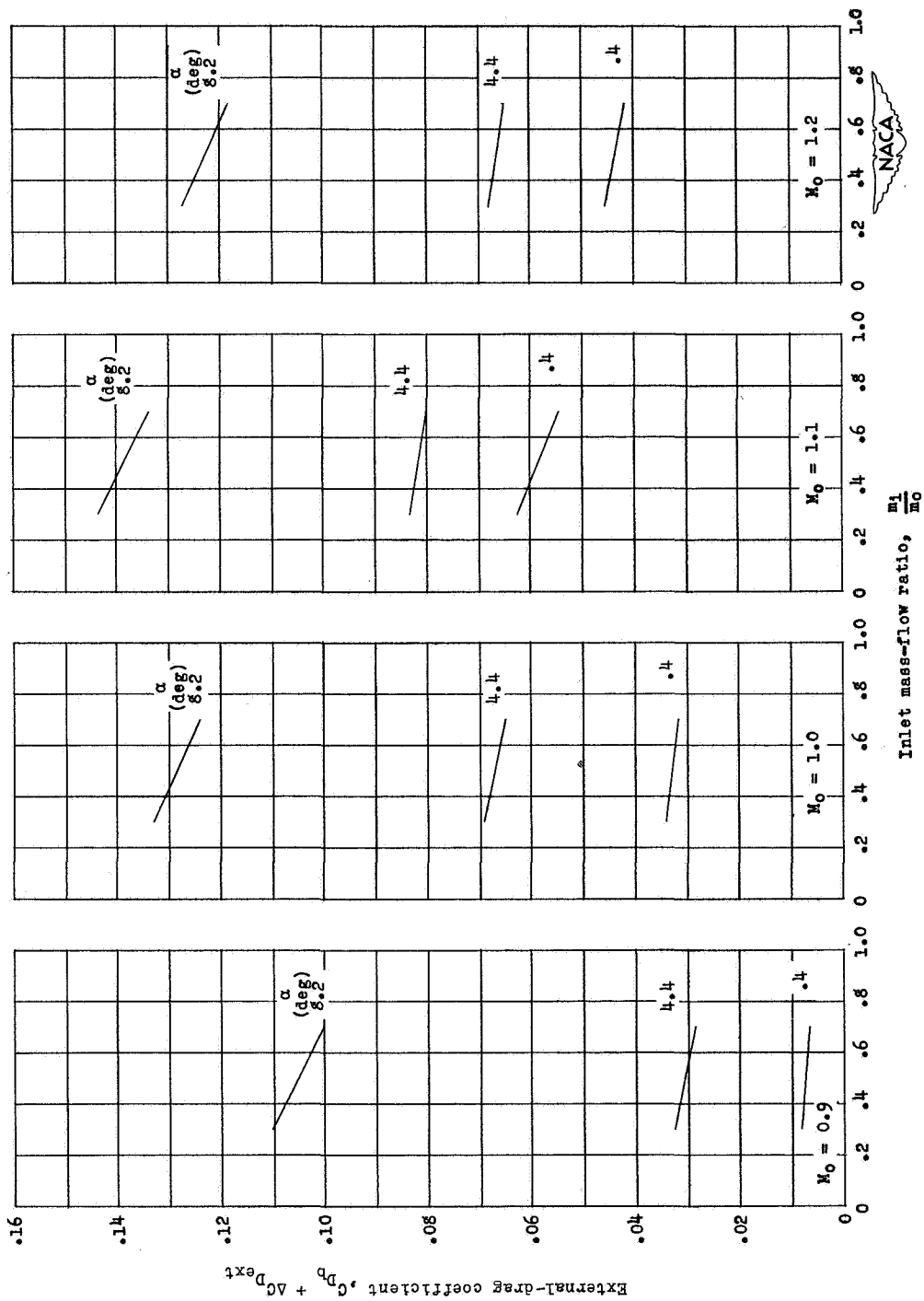

(c) Effect of mass-flow ratio.

Figure 12.- Concluded.

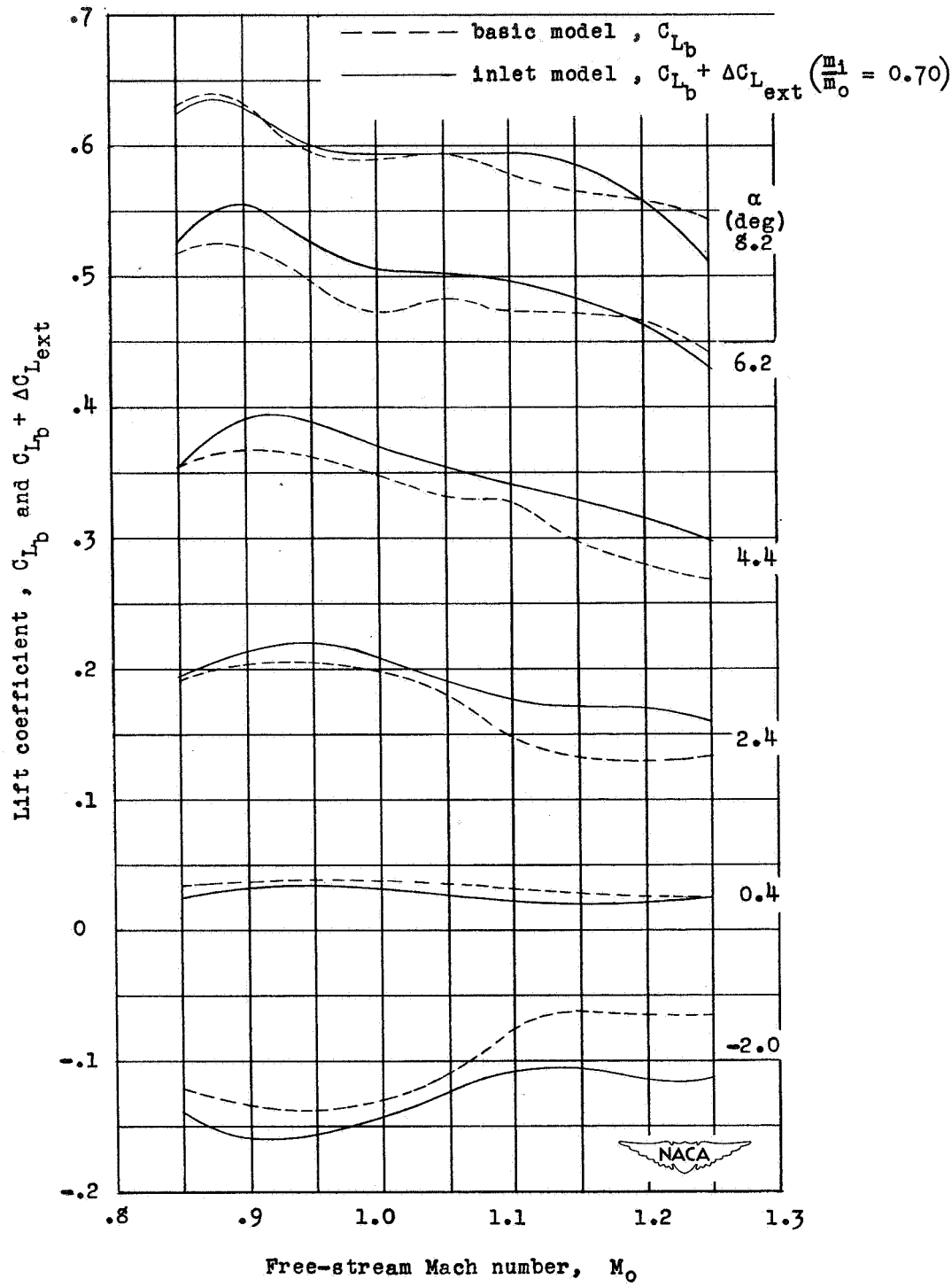

(a) Effect of Mach number.

Figure 13.- Effects of variations in Mach number, angle of attack, and mass-flow ratio on the lift coefficient.

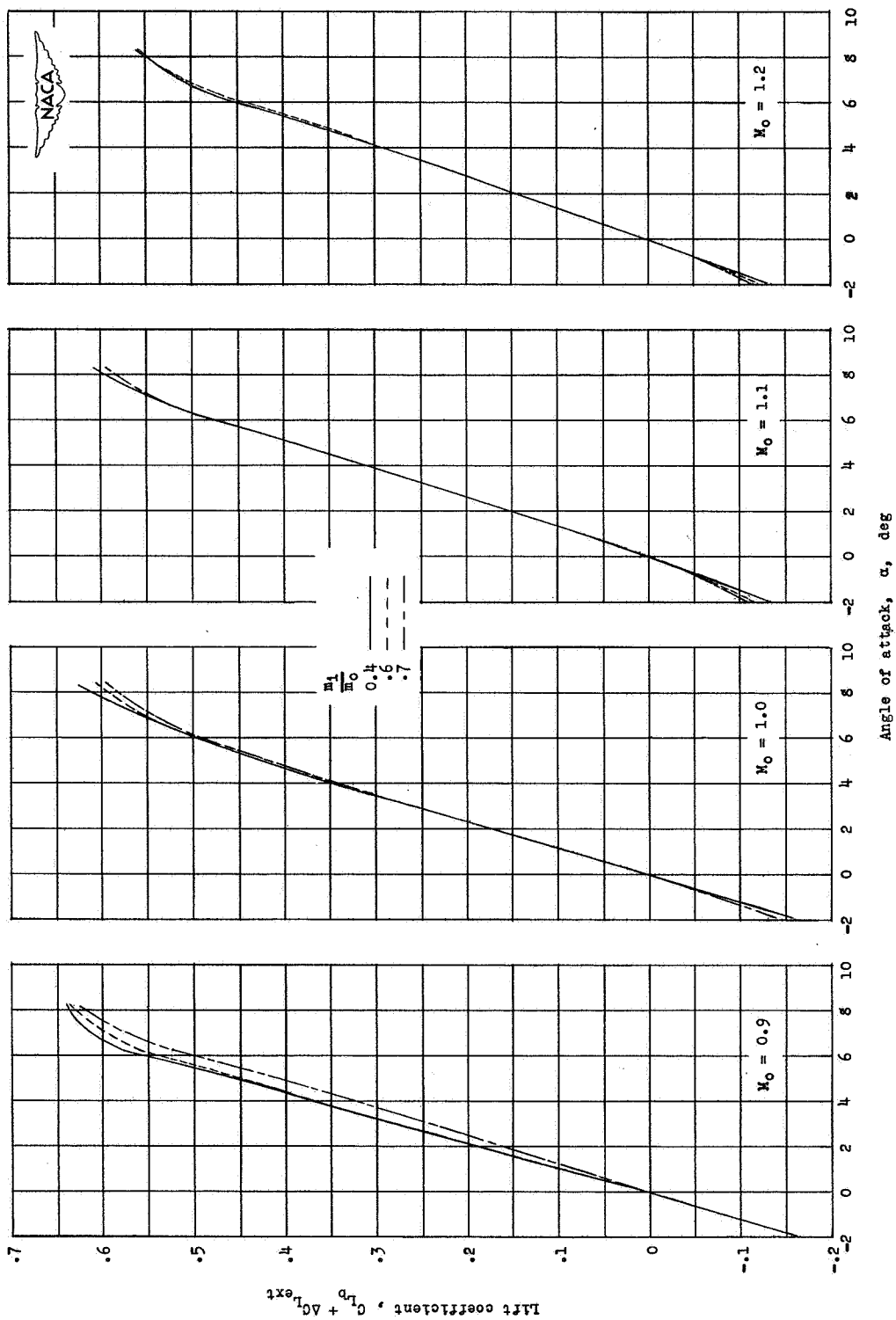

(b) Effects of angle of attack and mass-flow ratio.

Figure 13.- Concluded.

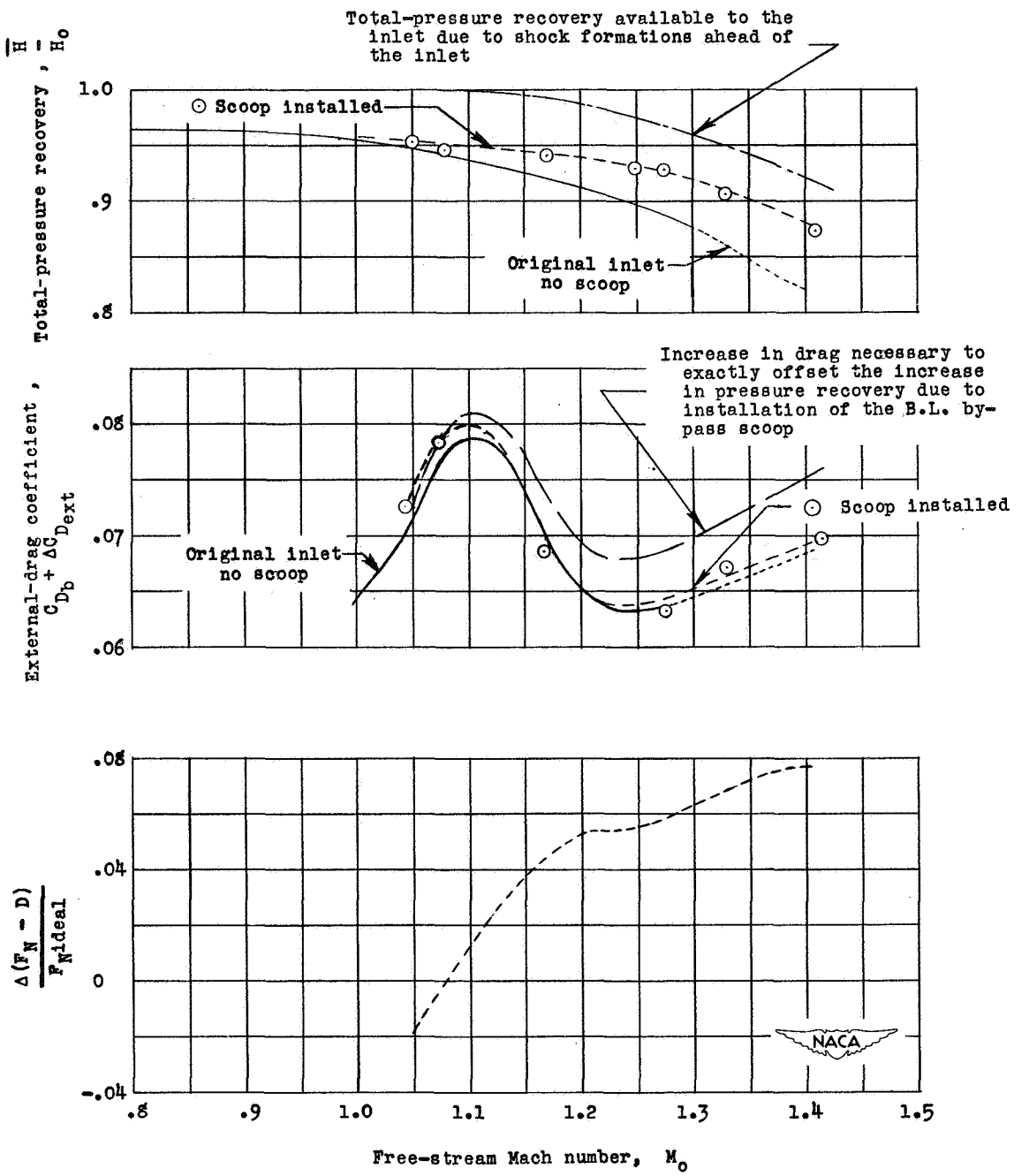

Figure 14.- The effect of fuselage-boundary-layer removal on the inlet performance. Maximum test mass-flow ratio condition; $\alpha = 4.4^{\circ}$.

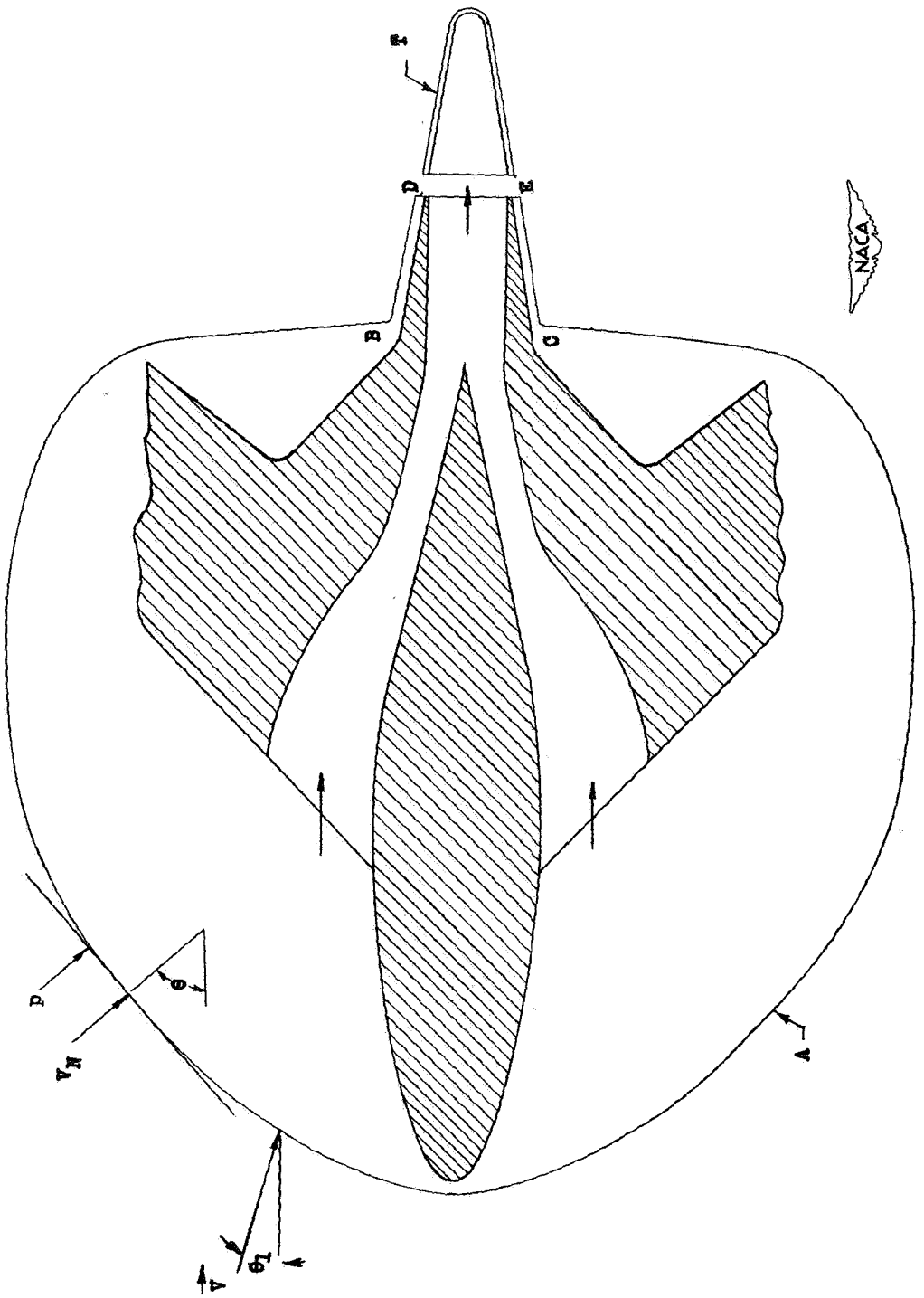

Figure 15.- Schematic diagram illustrating method of determining the external-drag increment of an air intake.

NACA-Langley - 10-1-52 - 325